The drawability of low carbon steel wire

Roger David Ian McCallum

Department of Mining and Metallurgical Engineering, Faculty of Engineering

McGill University Montreal

Submitted May, 1992

A thesis submitted to the Faculty of Graduate Studies and Research in partial fulfillment of the requirements of the degree of Master of Engineering.

Abstract

Four low carbon steels were drawn from rod to wire on a commercial multi-die wire drawing machine. Samples were obtained from between dies. Internal damage, as a function of cold work, was determined using precision density measurements. Nitrogen was observed to have the greatest effect on the ductility of low carbon steel. Interstitial nitrogen causes internal damage, which results in wire breaks. The mobility of nitrogen increases with temperature, which could account for the increased probability of wire breaks at high drawing speeds.

Quatre aciers à bas carbone ont été étirés de fil machine à fil au moyen d' une machine à fil de type commercial comprenant plusieurs filierès. Des échantillons ont été obtenus après chaque rétrécissement. Les endommagements internes, function du travail à froid, ont été déterminés en utilisant des mesures de densité précises. L'azote a la plus grande influence sur la ductilité des aciers à bas carbone. L'azote interstitiel cause des défauts internes qui résultent en bris du fil d'acier lors de l'étirage. La mobilité de l'azote augmente avec la température. Ce phénomène explique peut-être pourquoi la probabilité de rupture du fil d'acier augmente lorsque les vitesses d'étirage augmentent.

TABLE OF CONTENTS

ACKNOWLEDGEMENTS

I would like to acknowledge the support and co-operation of Ivaco Rolling Mills for providing the opportunity, the use of production facilities, and the steel used in the experiments. I would like to thank J.C. Legault and D. Peloquin of Sivaco Quebec for the use of their drawing facilities and help.

H. Campbell of McGill University provided assistance with electron microscopy and F. Paray with the Instron. A. Desilets of the Ecole Polytechnique made a precision balance available, and helped in the construction of the sample holding apparatus.

LIST OF SYMBOLS

A_0	Initial area
A_f	Final area
D_0	Initial diameter
D_f	Final diameter
F_i	Ideal deformation force
F_f	Force due to metal to die friction
F_r	Force of redundant reduction
F_s	Force to overcome internal shear
K	Constant
L_0	Initial length
L_f	Final length
R_0	Initial radius
R_f	Final radius
TM	Time metal is in the die
V_0	Initial velocity
V_f	Final velocity
V_l	Volume of displaced liquid
V_s	Volume of the steel sample
W_a	Weight of the object in air
W_i	Weight of the object immersed in the liquid
W_l	Weight of the displaced liquid
$f(\alpha)$	Shape factor
m	Strain rate sensitivity
n	Work hardening exponent
r	Fractional reduction of area

α	Die half angle
ε	True strain
$\dot{\varepsilon}$	True strain rate
η	Drawing efficiency factor
μ	Metal to die friction factor
ρ_l	Weighing liquid density
ρ_s	Density of steel sample
σ_{xf}	Applied draw stress
σ_0	Yield stress of the material
τ	Shear stress

INTRODUCTION

The North American steel industry has made a dramatic shift toward the production of steel from scrap over the past twenty years. In 1970, 30 metric tons of scrap were purchased for every 100 metric tons of steel produced. By 1986, that ratio had increased to 48 metric tons of scrap for every 100 tons of steel produced (1). The driving force behind this trend is economic. The capital cost per tonne of capacity of building a scrap based electric furnace facility is only 20% of the cost to produce a fully integrated, blast furnace BOF plant (2). In addition to lower capital cost, the energy required to produce a tonne of steel from scrap is typically about 40% of the total energy required to produce a tonne of steel from iron ore in a fully integrated steel mill (3).

As the trend toward the use of recycled steel has increased, so has the problem of nonferrous residual element concentration. The residual elements normally referred to are copper, nickel, chromium, molybdenum and tin. In addition to residual elements, steel makers are increasingly becoming aware of the deleterious effect of nitrogen to their product. The residual elements cannot be removed from steel at low cost on an industrial scale. Nitrogen is present in the air, and is found in some alloys and additions as a tramp element.

Steel processors are concerned about the effect of these elements on their productivity, and are beginning to restrict the maximum level of the residual elements in the steel which they order (4).

LITERATURE REVIEW

North American wire rod production in 1990 was 6.5 million metric tons (5). With the exception of a limited number of structural products which are cold rolled from rod, all steel wire rod is drawn through at least one die. This thesis is concerned with steel wire drawn about 90%. This eliminates from the study wire rod produced for cold heading applications, where the drawing operations performed are mainly used to size the wire prior to cold heading. Another class of steel eliminated from the study is high carbon steel, which typically undergoes a high percentage of cold deformation. The drawing characteristics of high carbon steel are, however, affected by the microstructure of the rod (6), as well as by the factors under investigation in this thesis. For this reason, low carbon steel was selected for study, in order to eliminate microstructrual effects from the results.

Figure 1: Wire drawing die nomenclature (7)

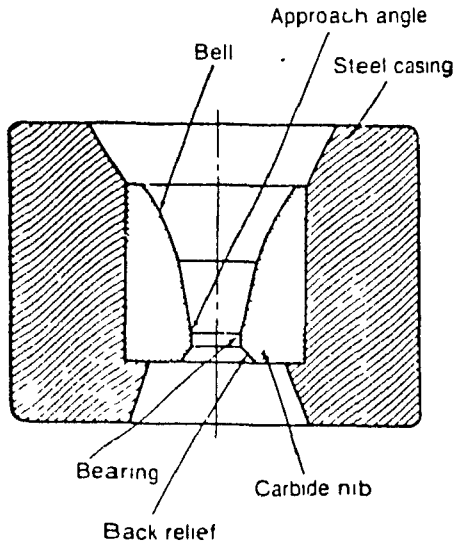

A wire drawing die, as illustrated in figure 1, consists of a bell entrance, which is useful when guiding new stock into a die during set up. The bell should not come into contact with the wire being drawn during normal operations. The approach is the part of the die where reduction of area takes place. The metal being drawn comes into contact with the die at a point between the beginning of the approach, and the bearing. This point is determined by the reduction of cross sectional area taking place in the die. The approach is also the part of the die in which the lubricant is pressed, compacted, and in some cases liquefied (8) on the wire surface. The angle of the die approach, or simply the die angle, is an important die characteristic. References to the die angle in this thesis are to the half angle of the die approach, rather than the full included angle.

The approach ends when the walls of the die become parallel to the centre line of the die, in the bearing. The bearing is also known as the die land. The purpose of the land, or bearing is to insure the finished wire is round, and has a smooth surface finish (9).

A major concern of industrial wire drawers is wire breaks. If steel wire breaks during drawing on a six die machine, lost time per break will be fifteen minutes, at a minimum, and can last up to an hour, depending on where the

break occurs. If wire breaks are frequent, the operator will be forced to reduce the drawing speed. If frequent wire breaks occur in the material supplied by one steelmaker only, productivity losses will force the wire drawer to find a new steel supplier.

Wire drawing breaks in low carbon steel are generally ductile in nature. Breaks which are not ductile can often be traced to large nonmetallic particles embedded in the rod, severe rolling defects, or a poor wire drawing arrangement (10). None of these defects will be considered in this work. The mechanism of ductile failure is well understood (10,11,12,13).

Ductile failure begins with the formation of microvoids in the metal matrix. As the material is strained, more microvoids nucleate, and grow. Further straining results in the coalescence of these microvoids. As the process continues, voids account for an increasing fraction of the total cross sectional area, until the remaining sound metal can no longer support the drawing load, and failure occurs.

Wire drawing models

Four models of the drawing process will be considered in

this thesis. Each makes it possible to examine a different aspect of the drawing process, and gain a better understanding of the factors which can lead to ductile failure.

The slip line field model is based on plane strain analysis, which can only be applied to two dimensional problems (14). Wire drawing cannot be modeled as a two dimensional system, but the process of sheet drawing is suitable for slip line field analysis, since for analytical purposes, the sheet can be considered as having infinite width, which allows one dimension to be ignored. The sheet drawing process serves as an analogy to wire drawing, and for that reason the analysis will be included in the discussion.

The velocity field model is used to approximate the wire drawing process. This model examines velocity changes in the die, and is used to study the dynamics of central burst failures.

The upper bound model examines the maximum possible balance between applied force and stress during wire drawing. This model allows the derivation of the maximum possible reduction of area that can take place in a wire drawing die. The model is based on a material which does not work harden (8), and as such cannot predict the response to multi-die

drawing.

A deformation model overcomes the short coming of the upper bound model, and allows the effect of work hardening and die efficiency to be examined.

Slip line field model

The forces responsible for ductile failure of wire during drawing can be understood by considering a model based on a 'rigid plastic material'. This hypothetical material is rigid if stressed below the yield point. It exhibits no elastic behavior. Once stressed beyond the yield point, it deforms plastically. Unlike real materials, a rigid plastic material will not work harden during plastic deformation (15).

In such a solid, it is possible to construct a geometric slip line grid, in such a way that hydrostatic pressures at nodal points can be numerically calculated (12,14,15). Such a series of slip lines for sheet drawing appears as figure 2.

Figure 2: Slip line field developed for sheet drawing (15).

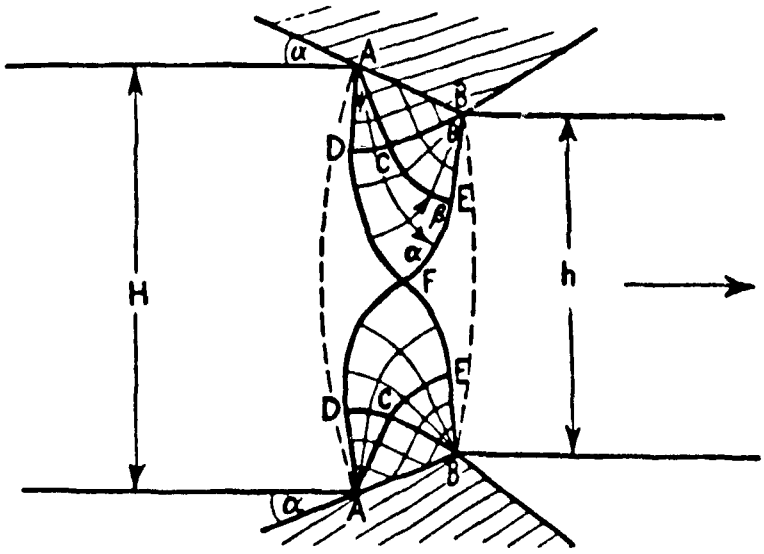

Slip line field analysis can be used to determine the numerical value of hydrostatic pressure at the centre of the sheet being drawn (12). A plot of these values is shown as figure 3.

Figure 3: Relative mid-plane hydrostatic pressure as a function of percent reduction of area and die to metal friction (12).

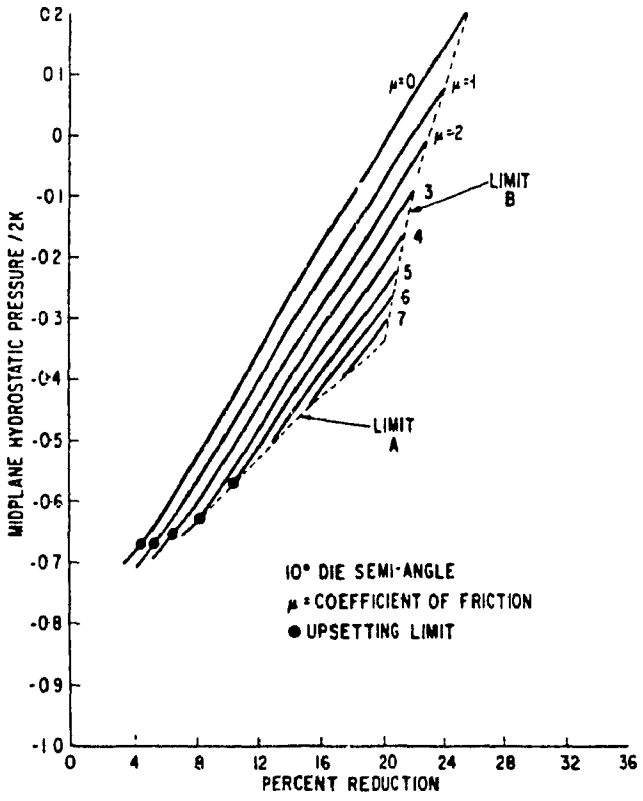

Figure 3 illustrates several important points. The mid-plane hydrostatic pressure is predominantly negative. This indicates that the mid-plane is in tension.

It is clear from figure 3, that for a given die angle, as the reduction of area decreases, the mid-plane tension rises. If die angle and reduction are held constant, the mid-plane tension rises as friction between the die and the wire is increased. Typical numerical values for metal to

die friction, using industrial wire drawing soap as a lubricant are near 0.02 (14,16).

Figure 3 refers to the upsetting limit, otherwise known as die entry bulging. Bulging occurs along with a high centre line tension, suggesting that the work of the die is restricted to the skin of the wire, and the majority of the drawing stress is felt as a tensile stress by the wire (10). Bulging and other undesirable flow patterns are illustrated by figure 4.

Figure 4: Schematic representation of undesirable flow patterns: bulging, converging and separation (8).

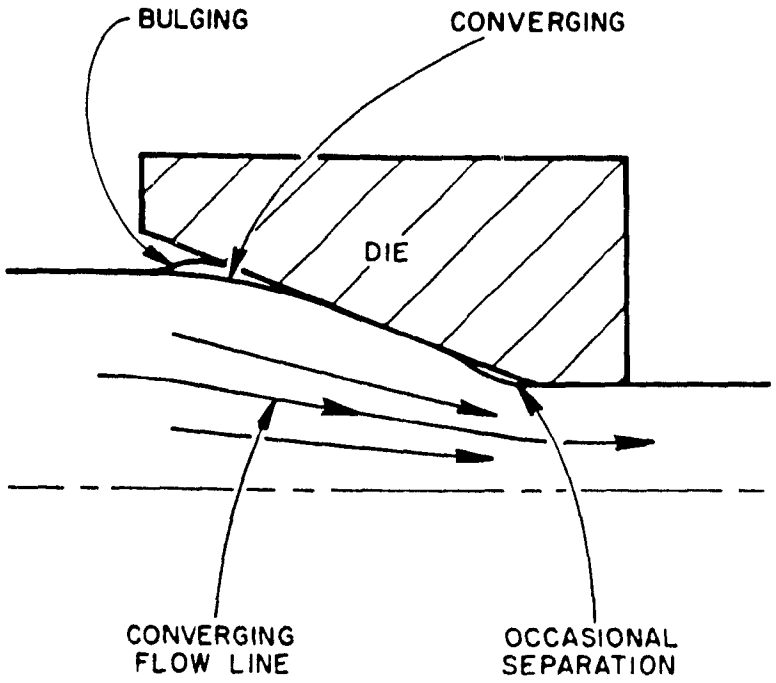

Figure 3 shows that it is theoretically possible to select a die angle and reduction of area such that there is no central tension, and that all the tensile stress exerted on the wire is transformed by the die into a compressive stress. Under these conditions, the possibility of nucleating or enlarging porosity does not exist (12).

Velocity field model

The velocity field model (17) provides another method to study wire drawing dynamics. The velocity field model is illustrated in figure 5.

Figure 5: Velocity field model of wire drawing (8).

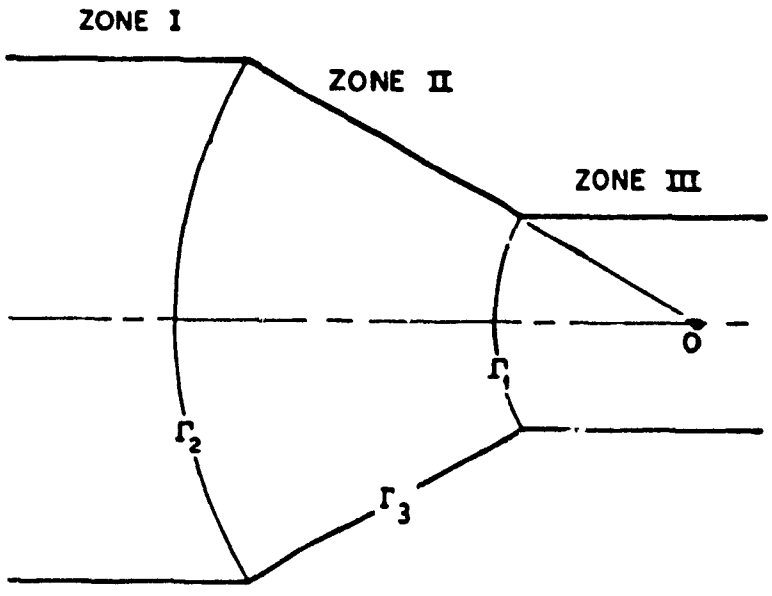

Figure 5 shows three distinct zones within the wire drawing die. Deformation takes place within the zone identified as Zone II. This zone is bounded by the surfaces Γ_1 Γ_2 and Γ_3. Γ_1 and Γ_2 are concentric spherical surfaces,whose origin is the imaginary point of convergence of the wire drawing die. Γ_3 is the surface of the truncated cone formed by the die, having an included angle of 2α.

Velocity discontinuities exist at the two spherical surfaces, Γ_1 and Γ_2. The velocity approaching surface Γ_2 is the initial velocity V_0, parallel to the drawing direction. The velocity of material leaving surface Γ_1 is V_f, the final wire velocity, and the direction is parallel to the drawing direction.

Figure 6: Velocity resolution in a wire drawing die (17).

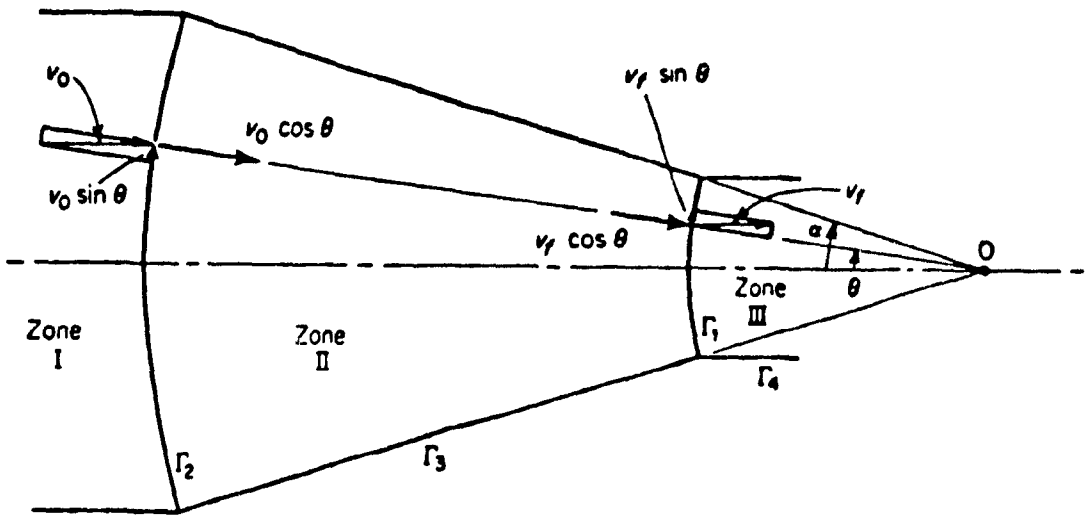

Figure 6 shows how the velocity crossing boundary Γ_2 is resolved to $V_0\cos(\Theta)$, where Θ is the angle which ranges from 0 to the half die angle α. The initial velocity, V_0 is resolved into $V_0\cos(\Theta)$, the velocity which converges at the theoretical point of die convergence, and $V_0\sin(\Theta)$, which is the component of the entrance velocity which is converted to shear. The shear component is greatest when $\Theta = \alpha$, and it is equal to zero, due to symmetry, at the centre.

The shear component is important to processes, such as wire drawing, which cause plastic flow. Plastic deformation, or yielding which occurs in a wire drawing die is caused by shear forces acting in the die. Pure tensile stress will not cause yielding (14).

The triaxial state of stress theory states that stress at any point in a material can be fully described by six components. Three normal stresses, designated σ_x, σ_y and σ_z, along with three shear stresses, designated τ_{xy}, τ_{xz} and τ_{yz} (7).

All stresses can be resolved onto three principal orthogonal axes, which need not correspond to the Cartesian x, y, and z axes. The principal stresses, are designated σ_1, σ_2, and σ_3. By convention, σ_1 has the greatest numerical

value, and σ_3 has the smallest value. It can be demonstrated (14) that the principal stress σ_1 during wire drawing is parallel to the drawing direction, along the centre line of the wire.

Tresca's criterion for plastic flow suggests that flow occurs when the maximum shear stress reaches a limiting value (14).

$$\tau_{max} = \frac{1}{2}(\sigma_1 - \sigma_3) \qquad (1$$

The surface of the rod is subjected to a greater shear stress than the center, and is, as a result, going to be subjected to the maximum shear stress and begin to flow before metal closer to the centre of the die.

Metal is subjected to increasing tensile forces, and less flow inducing shear forces as the center of the wire is approached. If the tensile forces approach the strength of the material, the effects will manifest themselves in the center of the wire before the outer surface is damaged. This accounts for the characteristic appearance of a ductile failure, in which the interior has failed through ductile mechanisms, while the skin fails in shear.

If the center of the wire is subjected to a tensile force equal to the failure stress, zone II will become non spherical, as illustrated in figure 7.

Sound flow occurs when zone II is continuous across the entire diameter of the rod. The phenomena of central bursting can be explained (8,18) by considering that Zone II is an annular region, which does not meet at the center line of the rod (AP 1).

Figure 7: Non spherical surface of a velocity discontinuity (8).

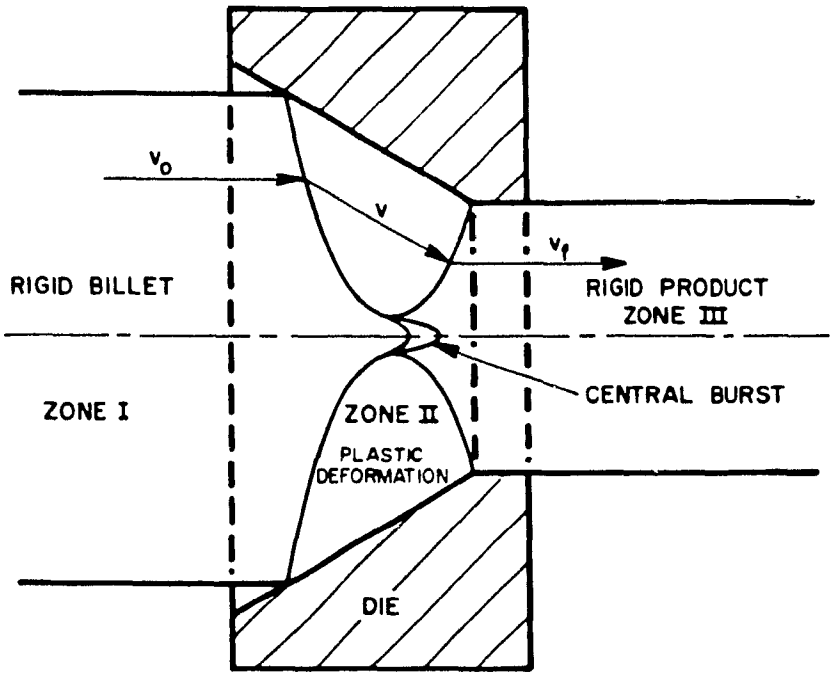

(AP 1) The appendix begins on page 83

When there is a velocity discontinuity between zone III and zone I, this discontinuity must be accommodated through the formation of a void. An explanation of the periodicity often observed in extreme cases of central bursting is presented as figure 8.

Figure 8: Model of central bursting periodicity (8).

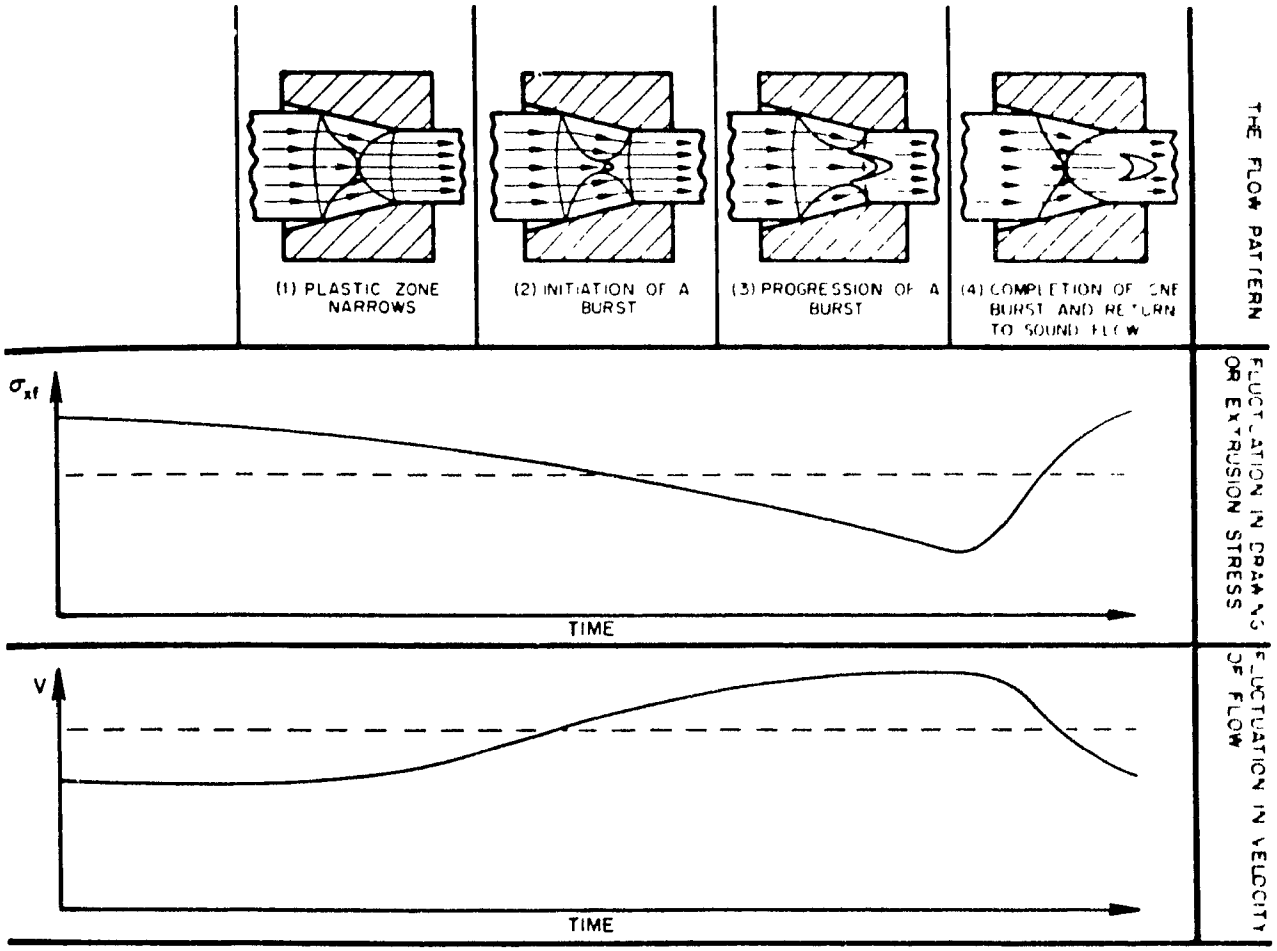

This analysis is based on the principle that central bursting takes place when the formation of a central burst requires less energy than sound flow (8).

Once nucleated, the metal behind the central burst will slow down, and approach the speed of zone I material, rather than maintain the velocity of zone III. When this occurs, there will be greater strain in the remaining annular zone II region. In a real material, this will result in increased work hardening. The work hardening would eventually arrest the propagation of the chevron. More material will be drawn through the die, and there will be a return to sound flow, before the cycle repeats.

Upper bound model

The internal forces which have been described using first the slip line field model, and the velocity field model can now be viewed within the context of the total stress required to draw wire through a die. There are three forces which must be overcome during wire drawing. For the purpose of this analysis, the force equations are normalized, or expressed as a fraction of the flow strength of the material.

There is the ideal force of deformation:

$$F_i = 2\ln\left(\frac{D_0}{D_f}\right) \qquad (2$$

This expression is called the ideal force of deformation, because it ignores any redundant work which takes place during metal forming operations (7). Since this is an ideal force, it is independent of the die angle.

The force of resistance to shear within the material:

$$F_s = \frac{2}{\sqrt{3}} \frac{\alpha}{\mathrm{Sin}^2(\alpha)} - \mathrm{Cot}(\alpha) \qquad (3$$

And the force required to overcome friction as the material flows through the die.

$$F_f = \frac{2}{\sqrt{3}} \mu \, \mathrm{Cot}(\alpha) \, \ln\left(\frac{D_0}{D_f}\right) \qquad (4$$

It will be noted that F_i, F_s and F_f, as they are defined in this model are dimensionless, and as such are not forces, but forces which have been normalized. The normalized forces can be added, to arrive at σ_{xf}, the applied draw stress, as a fraction of the yield stress of the material, σ_0.

$$\frac{\sigma_{xf}}{\sigma_0} = F_i + F_s + F_f \qquad (5$$

or

$$\frac{\sigma_{xf}}{\sigma_0} = 2f(\alpha)\ln\left(\frac{D_0}{D_f}\right) + \frac{2}{\sqrt{3}}\frac{\alpha}{\sin^2(\alpha)} - \cot(\alpha) + \frac{2}{\sqrt{3}}\mu\cot(\alpha)\ln\left(\frac{D_0}{D_f}\right) \quad (6$$

This is true for a die with no land. Resistance to flow through the land involves another expression which has been left out of this simple analysis. The analysis also assumes that back tension is zero, and ignores inertial forces (8).

Equations 2 through 6 are illustrated as figure 9

Figure 9: Contributions to total drawing stress (8).

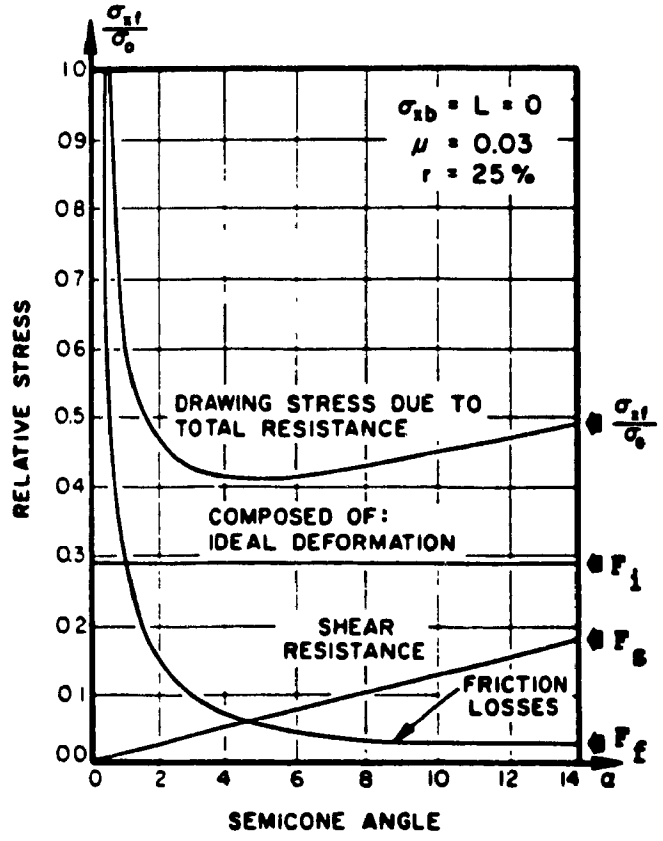

Figure 9 illustrates that for a given reduction of area, a small die angle results in a high friction contribution to flow resistance, up to the limit where the stress required to draw the material through the die exceeds the strength of the material, and the wire breaks outside the die (8).

As the die angle increases, the contribution of friction to the total force is reduced. At the same time, the amount of force required to overcome internal resistance increases. There is, for any given reduction of area, a die angle which will result in the minimum resistance to flow (8).

Equation 6 can be used to plot drawing stress as a function of die angle, for a number of reductions of area, to examine the variation of optimum die angles (17). This is shown as figure 10.

Figure 10: Relative drawing stress as a function of die angle and reduction of area (8).

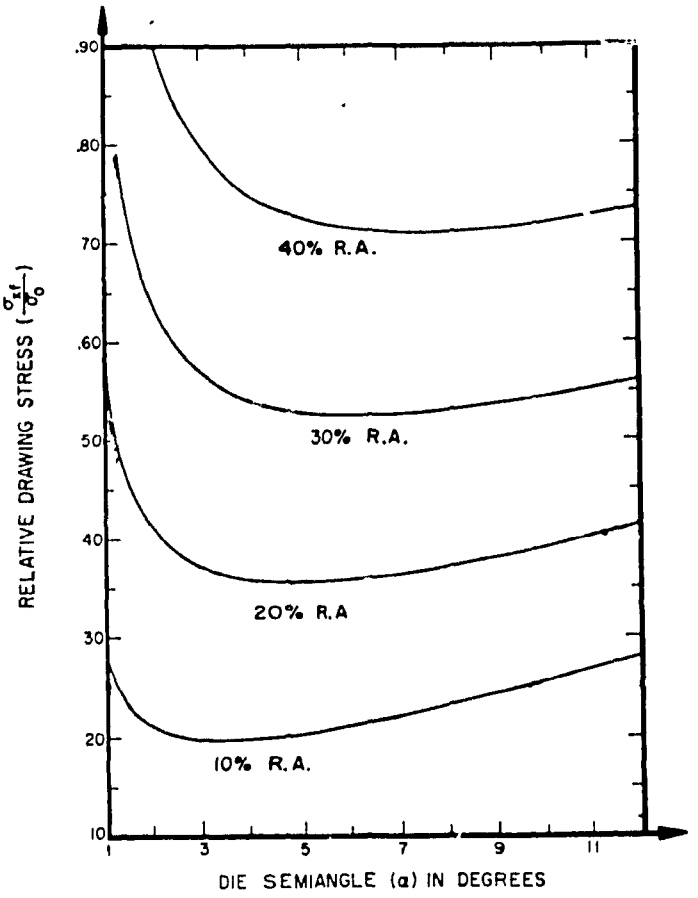

It is possible to determine the maximum theoretical reduction of area that can be made through a die. Since the drawing stress cannot exceed the flow strength of the material, the relation:

$$\frac{\sigma_{xf}}{\sigma_0} \leq 1 \qquad (7$$

must be true for all wire drawing processes.

The limit of

$$\frac{\sigma_{xf}}{\sigma_0} = 1 \qquad (8$$

can be expressed by re-writing equation 6.

$$\frac{R_0}{R_f} = \exp\left(\frac{\frac{\sigma_{xf}}{\sigma_0} + 1 - \frac{2}{\sqrt{3}}\left(\frac{\alpha}{\sin^2(\alpha)} - \cot(\alpha)\right)}{2\left(f(\alpha) + \frac{\mu}{\sqrt{3}}\cot(\alpha)\right)}\right) \qquad (9$$

Equation 9 is illustrated as figure 11

Figure 11: Maximum Reduction of Area Possible Through a Single Die as a Function of Die Angle and friction (18).

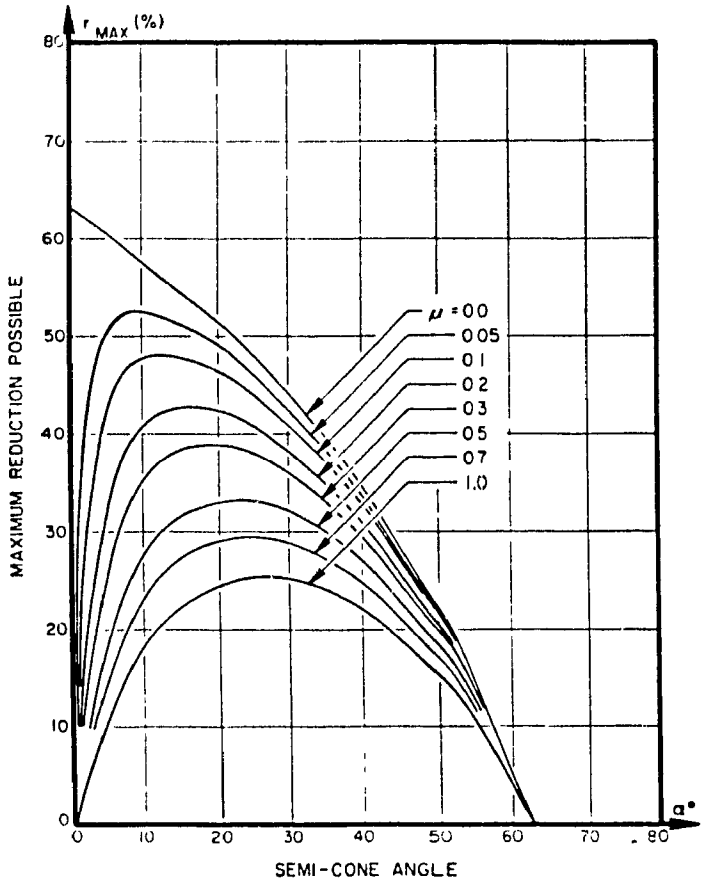

The value of μ is of the order of 0.02 in commercial wire drawing operations using soap as a lubricant (14,16). Figure 11 shows that it is theoretically possible to accomplish a 50% reduction of area through a die with a half angle of 6 to 10 degrees. This maximum possible reduction

occurs at a die angle which is close to the optimum die angle illustrated in figure 10.

Deformation model

Figure 11 was derived using the upper bound model, developed using a material in which work hardening was not considered (18). The deformation model (7), although not as detailed as the upper bound method, does allow a work hardening material to be analyzed.

First, consider the case of ideal plastic deformation

$$\sigma = \sigma_0 \ln\left(\frac{A_0}{A_f}\right) = \int \sigma d\varepsilon \qquad (10$$

The upper bound analysis separates the forces of wire drawing, as they are separated in equation 11, below.

$$F_t = F_i + F_f + F_r + F_s \qquad (11$$

In this case, the force to overcome redundant work, F_r is included. Redundant work was not included in the upper bound analysis.

An efficiency factor, η can be defined as F_i/F_t which takes into account metal to die friction, and redundant work. For the purpose of this analysis, these factors are considered to be constant. Typical values of η range from 0.30 to 0.60 (7).

The efficiency factor is used to modify equation 10 to

$$\sigma_{xf} = \frac{1}{\eta}\int \sigma d\varepsilon \qquad (12$$

since

$$\sigma = K\varepsilon^n \qquad (13$$

The draw block stress can be written

$$\sigma_{xf} = \frac{K}{\eta}\int \varepsilon^n d\varepsilon = \frac{K\varepsilon^{(n+1)}}{\eta(n+1)} = \frac{\sigma\varepsilon}{\eta(n+1)} \qquad (14$$

The point of necking outside the die will determine the maximum drawing load that can be applied, so

$$\sigma_{xf} = \sigma \qquad (15$$

Substituting equation 15 into equation 14,

$$\sigma = \frac{\sigma\varepsilon_{max}}{\eta(n+1)} \qquad (16$$

or, the maximum strain is expressed

$$\varepsilon_{max} = \eta(n+1) \qquad (17$$

Strain can be written:

$$\varepsilon = \ln\left(\frac{A_0}{A_f}\right) \qquad (18$$

so

$$\left(\frac{A_0}{A_f}\right)_{max} = \exp(\eta(n+1)) \qquad (19$$

Reduction is, by definition

$$r = 1 - \frac{A_f}{A_o} \qquad (20$$

So, the maximum reduction becomes, simply

$$r_{max} = 1 - \exp(-\eta(n+1)) \qquad (21$$

Equation 21 can be used to demonstrate that in the case where $\eta = 1$, meaning there is no metal to die friction or redundant work, and $n = 0$, or no work hardening takes place, then the maximum possible reduction in a single pass is 63%. In a real material, where there is work hardening, the maximum possible reduction increases. Equation 21 also shows

that as the efficiency of the process falls, due to friction and redundant work, the maximum possible reduction drops. This is consistent with the upper bound model, which is illustrated by figure 11.

Equation 21 can be used to provide some knowledge of a multiple reduction wire drawing operation. Examination of a true stress-strain graph, such as the one included in the experimental results as figure 17, page 59, shows that after each pass, the slope of the curve, which is related to the numerical value of n, decreases. This tells us that as strain accumulates in the wire, and the value of n falls, the maximum possible reduction in a die falls.

Both models predict a reduction of area considerably in excess of the uniform reduction of area which would be obtained during a tensile test. This prediction is consistent with observations. The confined deformation caused by a wire drawing die introduces a compressive stress, which promotes metal flow, and results in a greater reduction of area than would be obtained during a tensile test, where the induced transverse compressive stress is not present (7).

Internal damage

Voids in steel do not always appear as periodic central bursts, but the forces which cause central bursting will also

promote void nucleation, growth and coalescence, under different conditions. In a study of the tensile deformation of copper (19), it was found that voids first began to form at locations where the metal had the greatest difficulty conforming to the general flow pattern, such as at triple points.

In samples subjected to greater strains, voids were observed on grain boundaries which were roughly parallel to the stress axis. As the voids grew, they were able to concentrate strain, as if they were internal notches. This concentration of strain resulted in the development of discrete regions, or sheets of strain, which grew at an angle of about 30 degrees to the stress axis. The actual mode of failure was the growth and linking of these void sheets, in a zig-zag pattern through the interior of the sample, with the periphery failing in shear. The zig-zag pattern of linked void sheets gave the center portion of the wire its rough failure appearance, which is characteristic of ductile failure.

Measurement of internal damage

If, at any point prior to failure, the amount of internal damage in a wire could be measured, this would provide a useful measure of the drawability of the steel.

Examination of a sample by sectioning and polishing can provide a measure of internal damage. Prior to examination. the layer of metal smeared by the mechanical polishing process would have to be removed, so that the voids were not masked or filled in completely. Mechanical polishing typically smears about 1 μm of material (20,22). Using the technique of ion bombardment, this layer of smeared material can be removed (11,21,22,28). Such sample preparation allows the voids to be observed using either optical or electron microscope techniques. Microscopy has the disadvantage that only a very small, and perhaps unrepresentative area of the sample can be observed, without an exhaustive amount of work.

The amount of internal damage in a sample can be obtained as a bulk measurement by studying the variation in density as the material is wire drawn (11,13). The principle is simple. As a material is cold worked, microvoids nucleate, grow and coalesce, and finally result in the failure of the wire. A steel with a relatively large volume fraction of voids will be closer to failure than a steel which is relatively void free. The material close to failure will have a lower density than the sound sample.

EXPERIMENTAL METHOD

It is well known by drawing machine operators, that the probability of experiencing wire breaks is reduced by lowering the drawing speed. Reducing the drawing speed is used by an operator who does not have the option of selecting new drawing stock whenever he experiences wire breaks. During any trial of a new steel lot, or steel supplier, wire drawers will always quote the speed at which the material was processed. Since drawing speed is related to productivity, wire drawers place a lot of significance on drawing speed when selecting a steel supplier.

The fact that a "good" steel can be drawn more quickly than an inferior steel, suggests that there is a relationship between wire breaks and strain rate sensitivity. Tensile testing was performed, but no relationship was found between the chemical composition of the steel and the strain rate sensitivity. An inspection of Table 5, included as part of the experimental results, page 52, shows that the strain rates obtained during commercial drawing operations are two orders of magnitude greater than those employed in the laboratory using a tensile testing machine. Furthermore, during industrial wire drawing, the temperatures take several minutes to reach a steady state. Strain rate sensitivity is a strong function of temperature (7). A laboratory tensile

test, especially at high rates of strain is over before a steady state temperature can be achieved. For these reasons, efforts to measure the strain rate sensitivity were abandoned, in spite of evidence to suggest that strain rate sensitivity affects wire breaks.

Precision density measurements

The first set of experiments were conducted on heat A22671 at Sivaco Quebec. The main purpose of the tests was to verify the feasibility of the experimental technique.

The experimental results were encouraging, and three additional heats were selected for processing. The chemical analyses of all four heats appear as Table 1, page 48. The heats chosen for the experiments were selected because they represent the extremes of chemistries which one can expect in low carbon steels. The heats selected allowed an orthogonal experimental design to be employed, as schematically illustrated in table 2, page 49 (AP 2,3). This is not always possible within the constraints that the samples were obtained from a full scale commercial steelmaking operation, where elements generally considered to be deleterious to steel processing cannot be added or removed at the convenience of the experimenter.

One coil was selected from each of the three heats, T14111, B3683 and A2208. They were processed at Sivaco Quebec on October 25, 1990. The steel was acid cleaned and borax coated prior to the experimental run. All steels were drawn using sodium soap as a lubricant. This preparation and lubrication is the standard drawing practice at Sivaco Quebec. The author was present during the wire drawing operation. Drawing the three coils took ten hours. This amount of time was required due in part to the lengthy interruptions required to obtain samples.

During processing, wire breaks were experienced during the drawing of the coil from heat B3683. In all, three breaks occurred, near the end of the coil. All breaks occurred after the last die. Two immediately behind the die, and the third in a roll straightener which is part of the spooler that puts finished wire on carriers.

Samples were obtained by stopping the wire drawing machine, and cutting samples after each die. This process is very disruptive to the drawing operation, as it takes over an hour to re-string the wire drawing machine. Sample collection is relatively easy, since each die is followed by a motorized 0.48 m diameter drawing drum, which holds about 50 rings of wire. Samples were taken off the drawing drums.

Samples taken after every die were tensile tested at

Sivaco Quebec. From these results, a true stress-strain curve was calculated for each of the three steels. This was accomplished by plotting the offset yield strength against the true accumulated strain after each die. The graphs appear as Figures 17 to 19, pages 59 to 61. The data used to plot the graphs appear as Table 3, found on page 50.

The samples prepared for precision density measurement were not straightened. Wire removed during processing on a wire drawing machine is in the form of rings. The diameter of the ring is the same as the diameter of the motorized block which pulls the wire through the die. Three 4.5 cm long samples were obtained from each ring. The samples were cut from the 0 degree, 90 degree and 120 degree positions from the wire samples obtained from the drawing drums.

These samples were clamped in a vice with fiber jaw inserts. The ends were filed so that they had no sharp edges. The samples were sanded with 500 grit paper, followed by buffing paper, to remove any residual drawing soap. After preparation, the samples were washed in acetone, and stored in a clean acetone solution. Once the sanding had been completed, the samples were handled only with tweezers which were washed in acetone. Each set of three prepared samples was kept in a separate container filled with laboratory grade

acetone to prevent oxidation prior to the precision weighing.

Weighing was conducted on a Mettler H-64 balance located at the Ecole Polytechnique, in Montreal. The samples were weighed using the apparatus shown in figure 11. This apparatus consisted of a sample holder with two sample positions. The lower sample hooks, made from 0.33 mm diameter platinum wire, were always immersed in the weighing fluid, so that any surface tension effects would influence both the wet and dry weights, and could therefore be ignored.

Figure 11: Illustration of the sample holding apparatus used to perform precision density measurements.

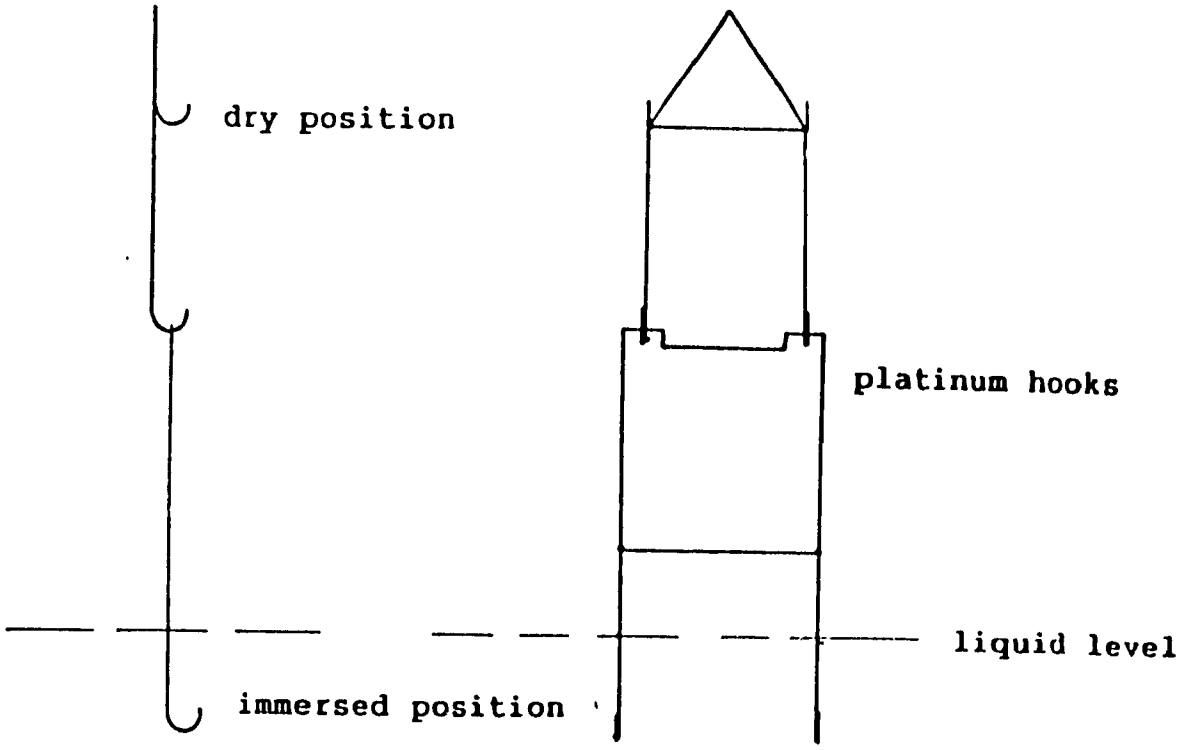

Samples were removed from the acetone, dried with an aerosol spray, and placed on the upper sample hooks. Repeat readings were taken, until the weights were reproducible Once a dry weight had been obtained, the balance was locked, and the sample removed with tweezers. The wet sample hook was lifted with a second pair of tweezers, to a rest position above the fluid. The sample which had just been weighed dry was placed on the wet hooks, while they hung in the rest position. Once in place, the wet hooks, containing the sample, were lowered into the fluid. A second reading was obtained. As in the case of the dry measurement, readings were taken until the balance had stabilized to give a reproducible reading.

Obtaining reproducible measurements when the balance stabilized was critical. The kinematic viscosity of the weighing fluid is 50 centistokes. As a comparison, the kinematic viscosity of water is of the order of 2 centistokes. The fact that the sample was immersed in a viscous fluid resulted in damping of the balance motion. Obtaining a correct weight with the sample immersed in oil typically took six to seven minutes. Numerous readings were obtained, and as the balance reached mechanical equilibrium, the difference from one reading to the next decreased, until there was no difference at all.

The weighing fluid used was a silicone oil, Rhodorsil 47V50, having a specific gravity of .959 at 25 C (23). This oil was recommended by F.Moussy of IRSID (24), and was selected because of its chemical inertness with respect to steel. The oil was degassed using an ultrasonic vibrating bath prior to the experimentation.

No specific precautions were made to control the temperature during the experiments. The experiments did not begin until the samples and fluid had stabilized at room temperature. The temperatures of the samples, the room and the weighing fluid were monitored after each set of three samples had been processed. All the temperatures were observed to be constant during the experiments.

Experiments were performed at the Ecole Polytechnique on January 31, 1991. Some data points required confirmation, and so a number of duplicate tests were made on June 13, 1991. At the same time, some samples from heat A22671 were weighed for the first time, so that data from that heat could be included as part of the thesis results.

Microscopic observations

The premise of the thesis is that the density differences observed are the result of internal damage caused

by cold work. This was confirmed by preparing some specimens for observation by scanning electron microscopy.

Sample preparation consisted of mounting wire samples longitudinally in bakelite. The bakelite thickness was measured, and the mounted specimens were sanded down until measurements showed that the samples had been sectioned to the center of the wire. The samples were hand sanded on progressively finer sandpaper, then finished with diamond polishing paste.

In order to remove the smeared layer, samples were broken out of the bakelite, cleaned in acetone and polished on an ion mill located in the McGill University Physics Building. Th ..oles were milled on one side only, although the mill is primarily designed to thin samples for transmission electron microscopy by milling both sides simultaneously.

The gun voltage was 6kV. The current was 0.75 ma. The gun was set at an angle of 20 degrees with respect to the sample, and the sample was rotated at 1 rpm. Each sample was bombarded with argon ions for one half hour.

The milled samples were examined on a scanning electron microscope located in the Department of Mining and

Metallurgical Engineering at McGill University. Photographs of the samples are presented as figures 12 to 15, found on pages 39 to 42.

Figure 12: Void formation around a spherical inclusion. Heat T14111, 4.70 mm diameter wire, 7500 magnification.

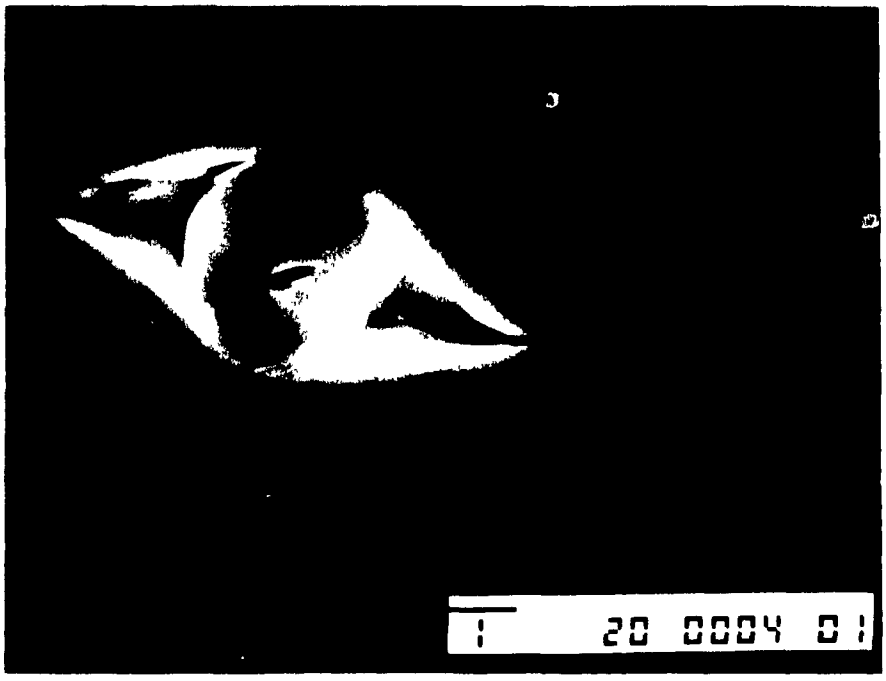

Figure 13: Void formation around a spherical inclusion. Heat T14111, 2.03 mm diameter wire. 5000 magnification.

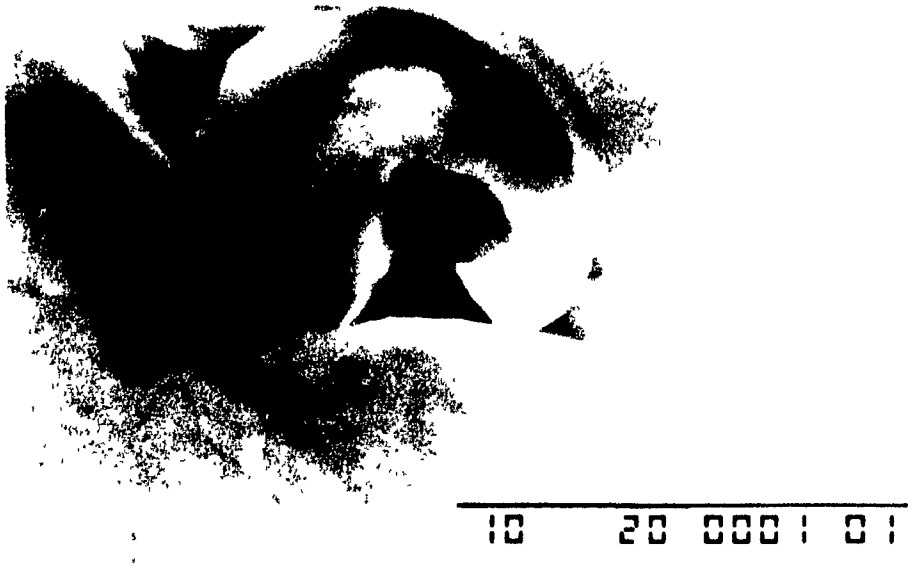

Figure 14: Void sheet formation. Heat B3683, 2.03 mm diameter wire. 7500 magnification.

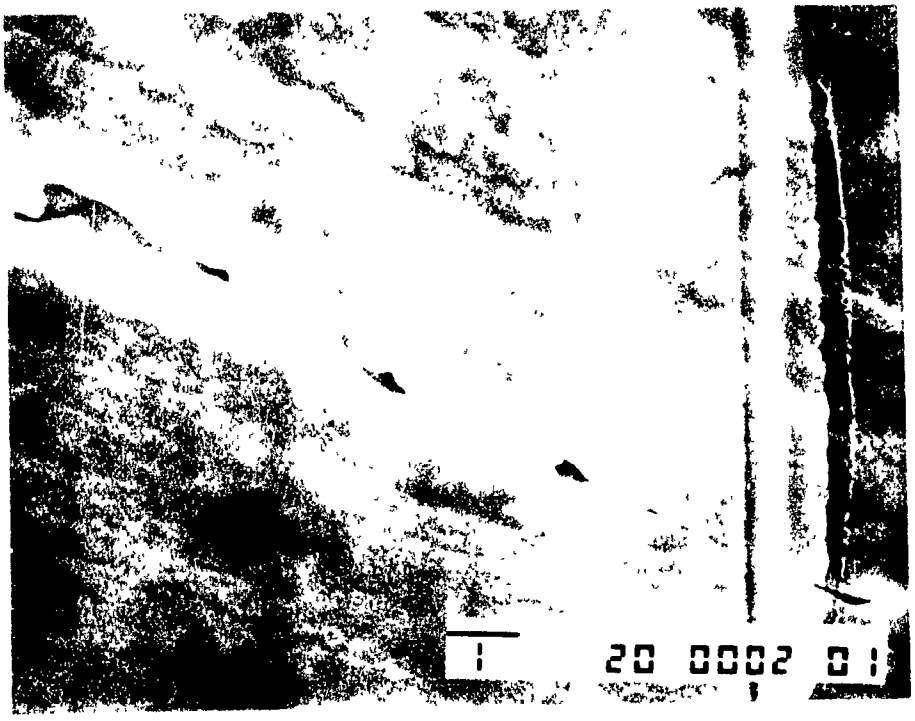

Figure 15: Void sheet formation in the vicinity of a wire break. Heat B3683, 2.03 mm diameter wire. 7500 magnification.

EXPERIMENTAL RESULTS

The true strain induced by each die and the velocity of the steel leaving each die were both calculated, so that strain rates could be derived. The finishing speed averaged 9.29 $m.s^{-1}$ during the processing of all three coils. Finishing speed is the velocity at which the finished wire leaves the last die on the machine.

True strain is given by the formula:

$$\varepsilon = \ln\left(\frac{A_0}{A_f}\right) \qquad (22$$

since

$$A = \frac{1}{4}\pi D^2 \qquad (23$$

then

$$\varepsilon = 2\ln\left(\frac{D_0}{D_f}\right) \qquad (24$$

Equation 24 was used to calculate the true strain per die, leading to the results shown in Table 4.

Once the strain per die is available, velocities can be

calculated backward from the finishing speed. Since:

$$\varepsilon = \ln\frac{(L_f)}{(L_0)} \qquad (25$$

then

$$L_0 = \frac{L_f}{\exp(\varepsilon)} \qquad (26$$

length can in turn be converted into velocity by dividing by unit time

$$V_0 = \frac{V_f}{\exp(\varepsilon)} \qquad (27$$

Equation 27 was used to calculate the exit velocities, which are listed in Table 4.

The average strain rate per die can be calculated as:

$$\bar{\dot{\varepsilon}} = \frac{\varepsilon}{(TM)} \qquad (28$$

where TM, the time a volume of metal remains in the die is:

$$TM = \frac{\text{volume in die}}{\text{volume flow rate}} \qquad (29$$

The volume of metal in the die can be calculated by considering that volume as the frustum of a cone. The

equation for calculating this volume is:

$$V = \frac{1}{3} (A_1 + A_2 + \sqrt{A_1 \cdot A_2}) h \quad (30$$

where:
A_1 = base area
A_2 = top area
h^2 = distance between top and bottom
V = volume

The distance h can be calculated by considering Figure 16.

Figure 16: Illustration of calculation used to determine the length of the deformation zone.

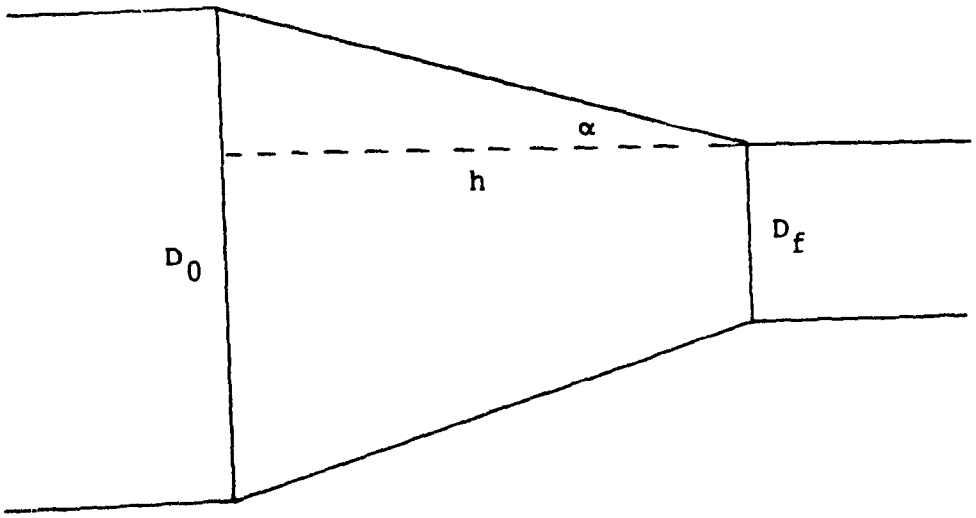

The value of h, the length of the deformation zone, is given as:

$$h = \frac{(D_0 - D_f)}{2} \cot(\alpha) \qquad (31$$

The volume flow rate is given by:

$$\text{Volume flow rate} = A_0 \cdot V_0 = A_f \cdot V_f \qquad (32$$

Equations 25 to 32 were used to calculate the strain rate per die; these are collected and shown in Table 5, page 52.

Density measurements

The density calculations are based on Archimedes principle, which states that the weight of the displaced liquid, W_l equals the weight of the object in air, W_a, less its immersed weight, W_i.

$$W_l = W_a - W_i \qquad (33$$

so

$$V_l \rho_l = W_a - W_i \qquad (34$$

Since the volume of the displaced liquid is equal to the

volume of the object which displaces the liquid, then:

$$V_l = V_s = \frac{W_a}{\rho_s} \qquad (35$$

Substituting equation 34 into equation 35, and rearranging leads to:

$$\rho_s = \frac{W_a \cdot \rho_l}{(W_a - W_i)} \qquad (36$$

Equation 36 was used to calculate the individual densities, which are listed in Tables 6 through 9, pages 53 to 56. Some data points were considered rogue points, and were excluded from subsequent analyses. These points do, however, appear in Tables 6 through 9 in brackets.

Tables 10 and 11, pages 57 and 58, were calculated from the data listed in Tables 6 through 9. These results have been plotted, and are presented as figures 21 to 24, pages 63 to 66.

Table 1: Chemical analyses of the steels used for the experimental work. All analytical values are expressed as weight percent.

Element	T14111	B3683	A2208	A22671
C	0.07	0.10	0.06	0.06
Mn	0.52	0.49	0.48	0.45
P	0.12	0.008	0.009	0.006
S	0.007	0.008	0.026	0.016
Si	0.14	0.03	0.11	0.12
Cu	0.03	0.07	0.19	0.25
Ni	0.07	0.04	0.07	0.10
Cr	0.04	0.03	0.07	0.09
Mo	0.01	0.02	0.02	0.02
Sn	0.004	0.010	0.010	0.060
Al	0.008	0.006	0.006	0.005
O	0.0064	0.0068	0.0107	0.0200
N	0.0036	0.0115	0.0074	0.0091
Ca	0.0024	0.0025	0.0004	n/a

Table 2: Data orthogonality

Heat	Cu	S	Sn	N
T14111	0	0	0	0
B 3683	0	0	0	1
A 2208	1	1	0	1
A22671	1	0	1	1

Table 3: Data used to calculate the true stress strain-curves for three of the experimental steels; true strain, and offset yield stress after each die.

Diameter (mm)	ε	Offset Yield B3683 (MPa)	Offset Yield T14111 (MPa)	Offset Yield A2208 (MPa)
5.50(rod)	-	-	-	-
4.70	0.32	620	565	586
4.01	0.64	710	662	689
3.43	0.95	765	717	744
2.97	1.24	827 827	765	779
2.59	1.51	882 896	813	834
2.29	1.76	910 910	813	848
2.03	2.00	910 930	827	868

Note: due to the unusually high values obtained for heat B3683, duplicate tests were performed on the last four samples.

Table 4: True strain per die, and drawing velocities

Diameter (mm)	Area (mm^2)	Strain per die	Velocity ($m.s^{-1}$)
5.50(rod)	23.42	0	1.24
4.70	17.35	.319	1.73
4.01	12.65	.316	2.36
3.43	9.23	.315	3.25
2.97	6.97	.286	4.35
2.59	5.29	.274	5.72
2.29	4.12	.250	7.34
2.03	3.22	.263	9.29

Table 5: Wire Drawing Strain Rates

Entry diameter (mm)	Die half angle (degree)	Length in die (mm)	Volume in die (cm^3)	Time in die ($s \times 10^2$)	Strain rate (s^{-1})
5.50(rod)	6	3.63	7.37	0.25	128
4.70	6	3.25	4.85	0.16	198
4.01	6	2.77	3.33	0.11	286
3.43	6	2.16	1.95	0.05	572
2.97	4	2.72	1.66	0.05	548
2.59	4	2.18	1.02	0.03	833
2.29	4	1.83	0.67	0.02	1180

Table 6: Heat A26671 density measurements

Wire size	5.50(rod)	4.60	3.83	3.23
R of A (%)	-	31	52	66
ε	-	0.37	0.73	1.08
		7.85863		7.84595
				7.84216
				7.84659

Wire size	2.74	2.36	2.03
R of A (%)	75	82	87
ε	1.40	1.70	2.00
	7.85577		7.85080
	7.84916		7.80876
			7.84689

Table 7: Duplicate heat A26671 density measurements

Wire size	5.50(rod)	4.60	3.83	3.23
R of A	-	31	52	66
ε	-	0.37	0.73	1.08
		7.84870	7.83676	
		7.84658	7.84070	

Wire size	2.74	2.36	2.03
R of A	75	82	87
ε	1.40	1.70	2.00
	7.83074	7.82209	
	(7.81798)	7.82952	
		7.82610	

Data points which have been ignored are bracketed (---)

Table 8: Individual density measurements

Wire size	5.50(rod)	4.70	4.01	3.43	2.97
R of A	-	27	47	61	71
ε	-	0.32	0.64	0.95	1.24
T14111		7.84276	7.85253	7.84847	7.84650
		7.84204	7.86007	7.85562	7.86226
		7.83980	7.86459	7.84041	7.85547
B3683		7.84573	7.86472	7.85816	7.82866
		7.85730	7.85461	7.85079	7.84642
		7.85623	7.85132	7.83712	7.84561
A2208		7.85181	7.85652	7.84718	7.85145
		7.85599	7.84855	7.83396	7.84739
		7.85461	7.84794	7.84415	7.85102

Wire size	2.59	2.29	2.03
R of A (%)	78	83	86
ε	1.51	1.76	2.00
T14111	7.84851	7.84294	7.86871
	(7.87028)	7.84104	7.86703
	7.84327	7.84221	7.83683
B3683	7.84952	7.84599	7.83094
	7.83909	7.85788	7.82587
	7.86159	7.84170	(7.86125)
A2208	7.83834	(7.86169)	7.81900
	7.83528	7.83346	7.81957
	7.84157	7.83578	7.81418

Data points which have been ignored are bracketed (---)

Table 9: Duplicated density measurements

Wire size	5.50(rod)	4.70	4.01	3.43	2.97
R of A (%)	-	27	47	61	71
ε	-	0.32	0.64	0.95	1.24
T14111		7.84822 7.84904			
B3683		7.86480 7.85012			

Wire size	2.59	2.29	2.03
R of A (%)	78	83	86
ε	1.51	1.76	2.00
T14111		7.83015 7.83672	(7.81424) 7.84633 7.85344
B3683			7.80585 7.81831 (7.85674)

Data points which have been ignored are bracketed (---)

Table 10: Average values with rogue points removed.

Wire size	5.50(rod)	4.70	4.01	3.43	2.97
R Of A (%)	–	27	47	61	71
ε	–	0.32	0.64	0.95	1.24
T14111					
average		7.84437	7.85906	7.84816	7.85474
standard dev.		0.00405	0.00609	0.00761	0.00791
observations		5	3	3	3
B3683					
average		7.85484	7.85688	7.84869	7.84023
standard dev.		0.00729	0.00698	0.01068	0.01002
observations		5	3	3	3
A2208					
average		7.85414	7.85100	7.84176	7.84995
standard dev		0.00214	0.00478	0.00692	0.00222
observations		3	3	3	3

Wire size	2.59	2.29	2.03
R of A (%)	78	83	86
ε	1.51	1.76	2.00
T14111			
average	7.84589	7.83861	7.85445
standard dev.	0.00371	0.00531	0.01359
observations	2	5	5
B3683			
average	7.85007	7.84852	7.82024
standard dev.	0.01126	0.00838	0.01091
observations	3	3	4
A2208			
average	7.83840	7.83462	7.81758
standard dev	0.00315	0.00164	0.00296
observations	3	2	3

Table 11: Average values with rogue points removed

Wire size	5.50(rod)	4.70	4.01	3.43
R of A (%)	-	31	52	66
ε	-	0.37	0.73	1.08
A22671				
average		7.85130	7.84764	7.84490
standard dev.		0.00643	0.00150	0.00239
observations		3	2	3
Wire size		2.29	2.59	2.03
R of A (%)		75	82	87
ε		1.40	1.70	2.00
A22671				
average		7.84522	7.82590	7.83547
standard dev.		0.01297	0.00372	0.02322
observations		3	3	3

True stress vs true strain

figure 17 T14111

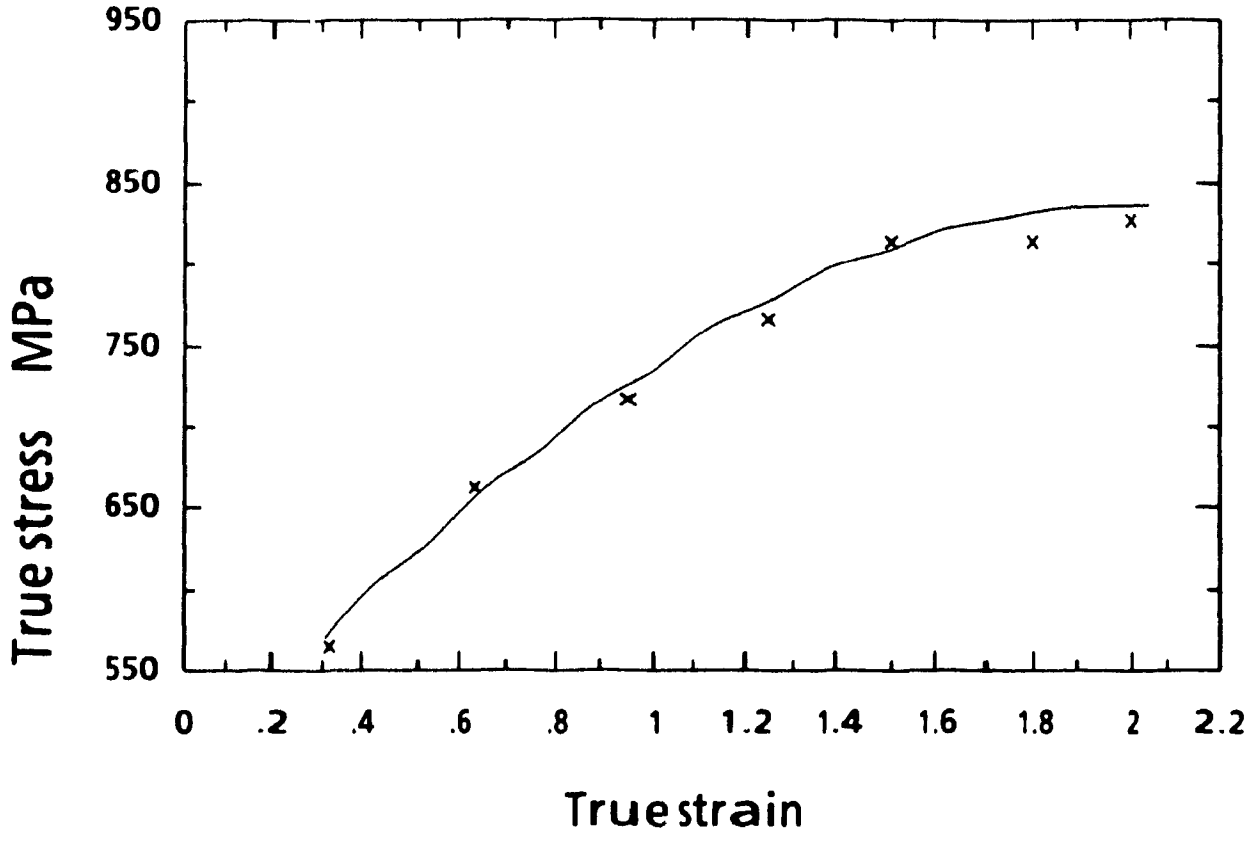

True stress vs true strain

figure 18 B3683

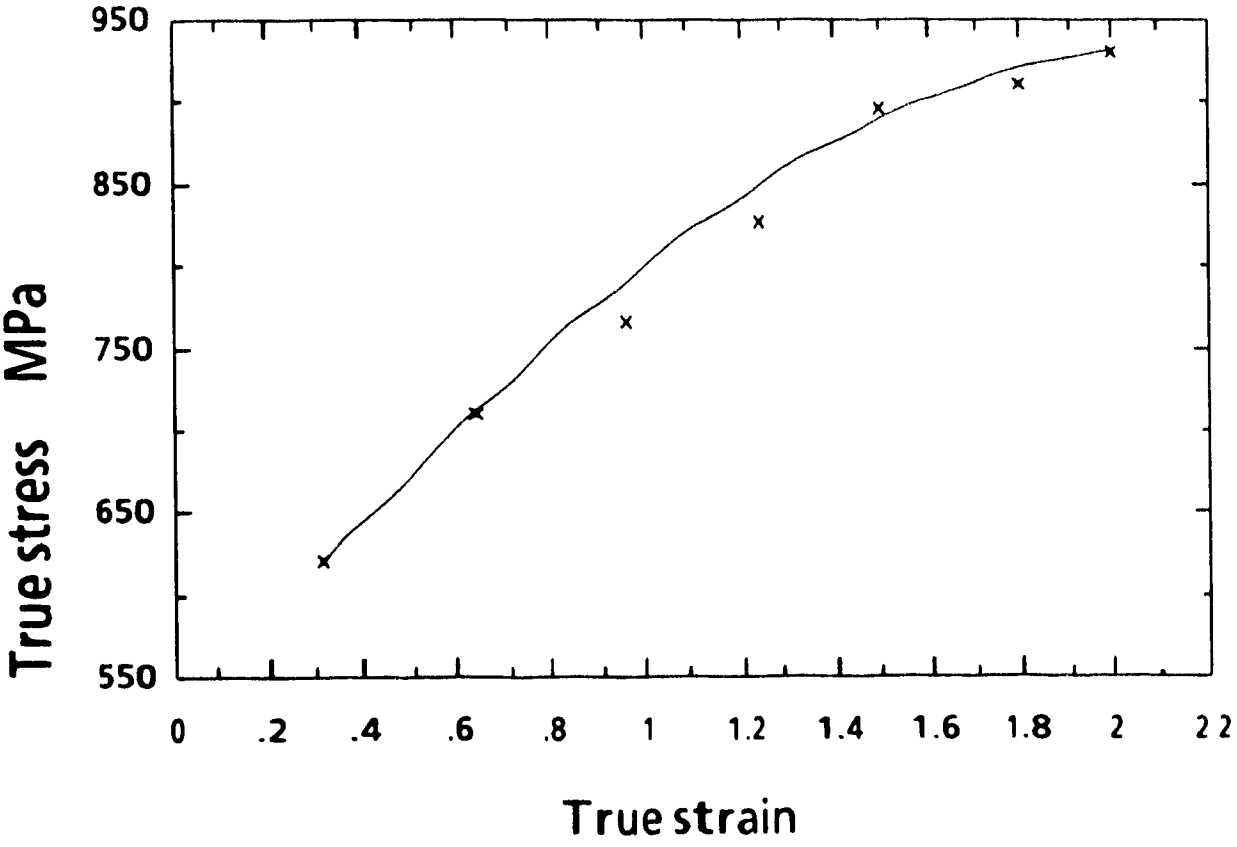

True stress vs true strain
figure 19 A2208

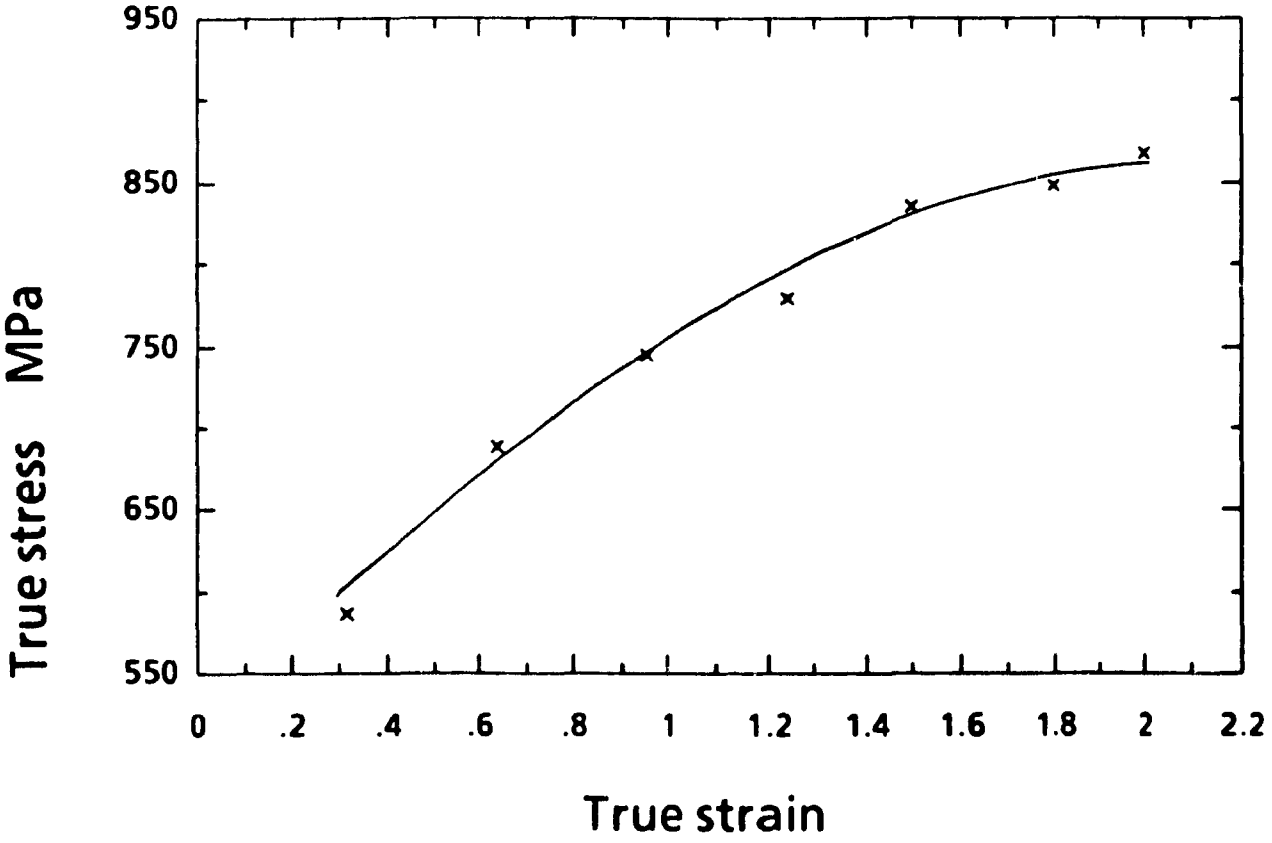

True stress vs true strain
figure 20 comparison of steels

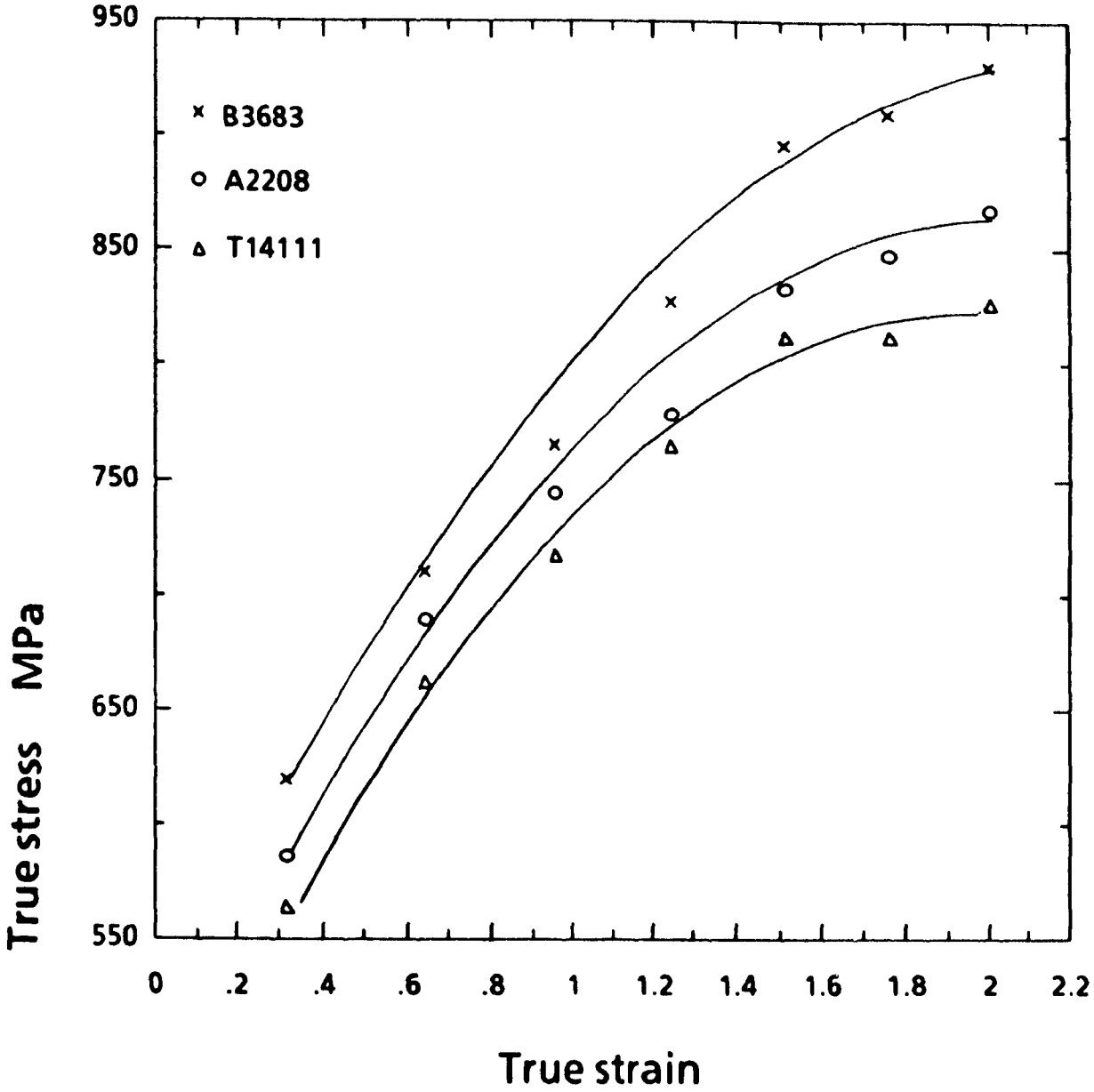

Density vs true strain
figure 21 T14111

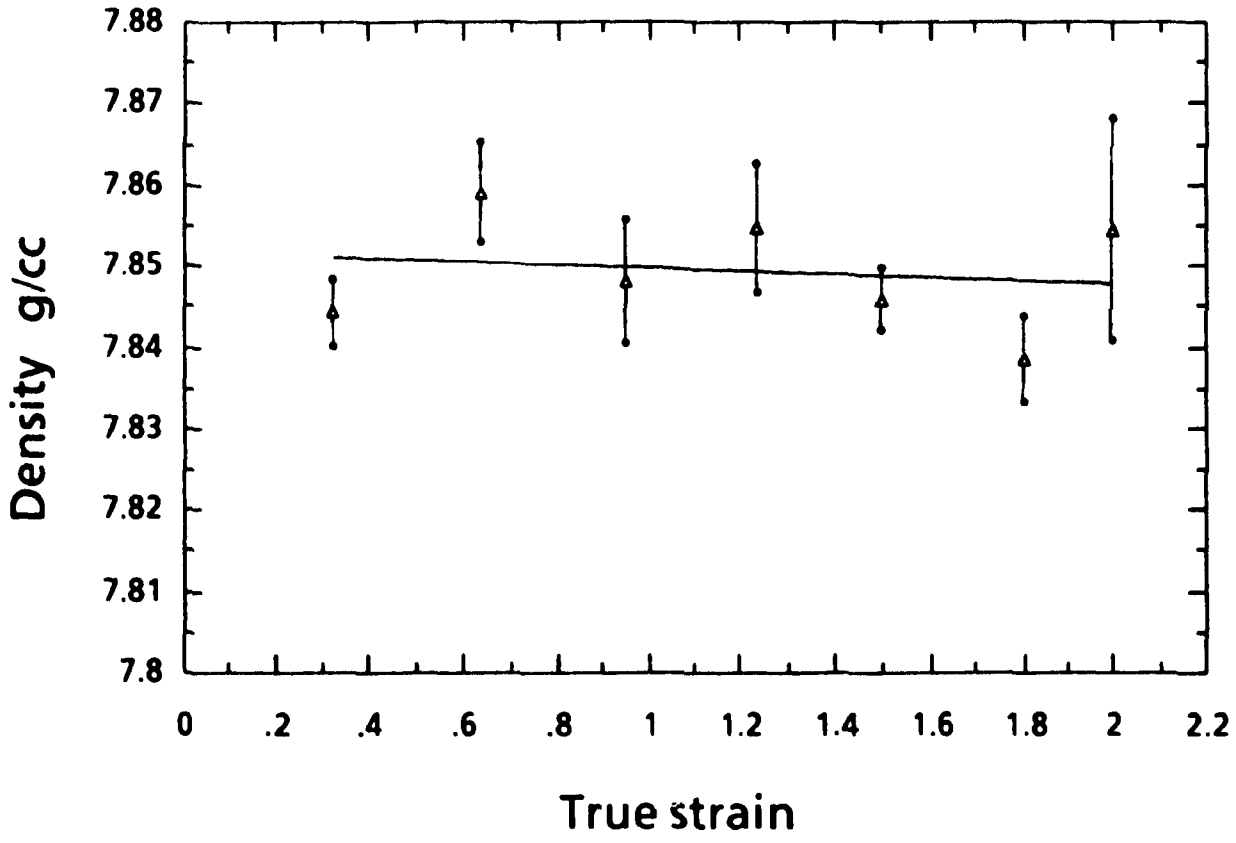

Density vs true strain

figure 22 B3683

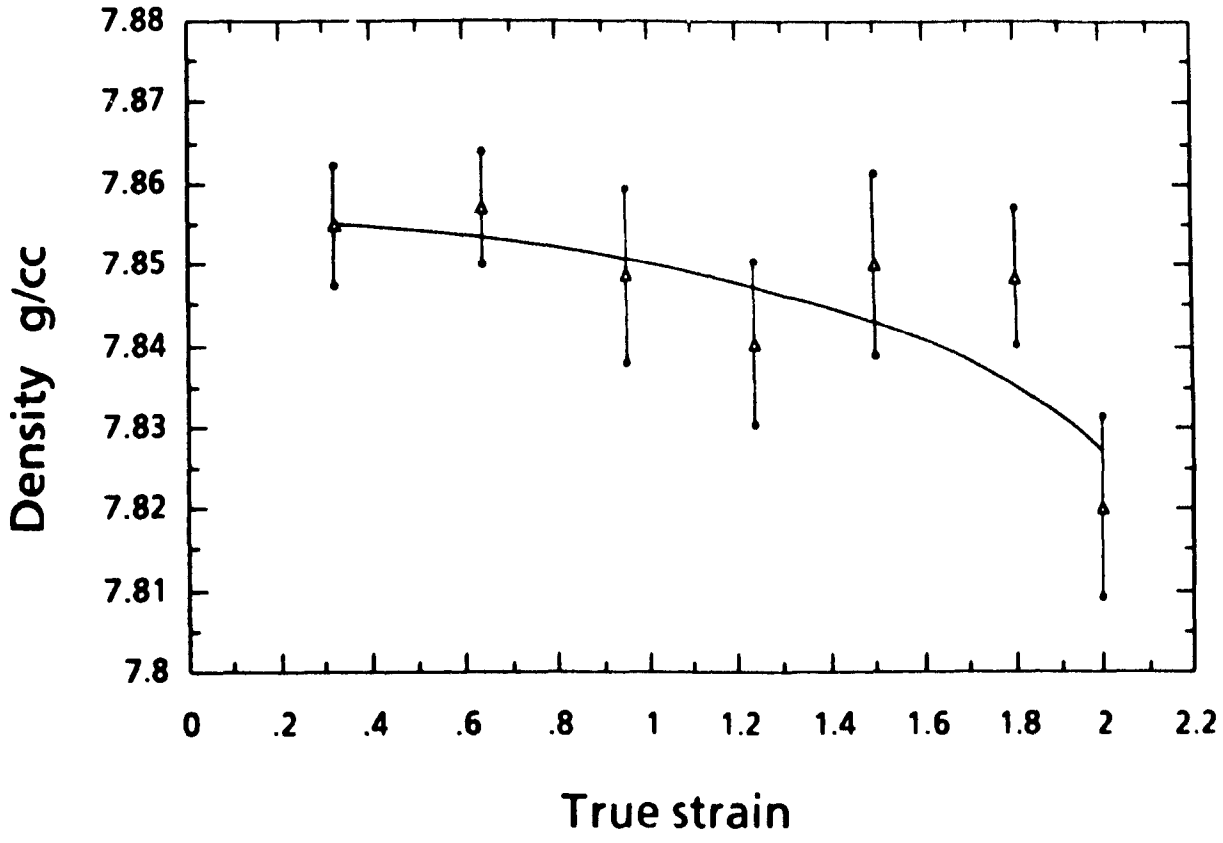

Density vs true strain
figure 23 A2208

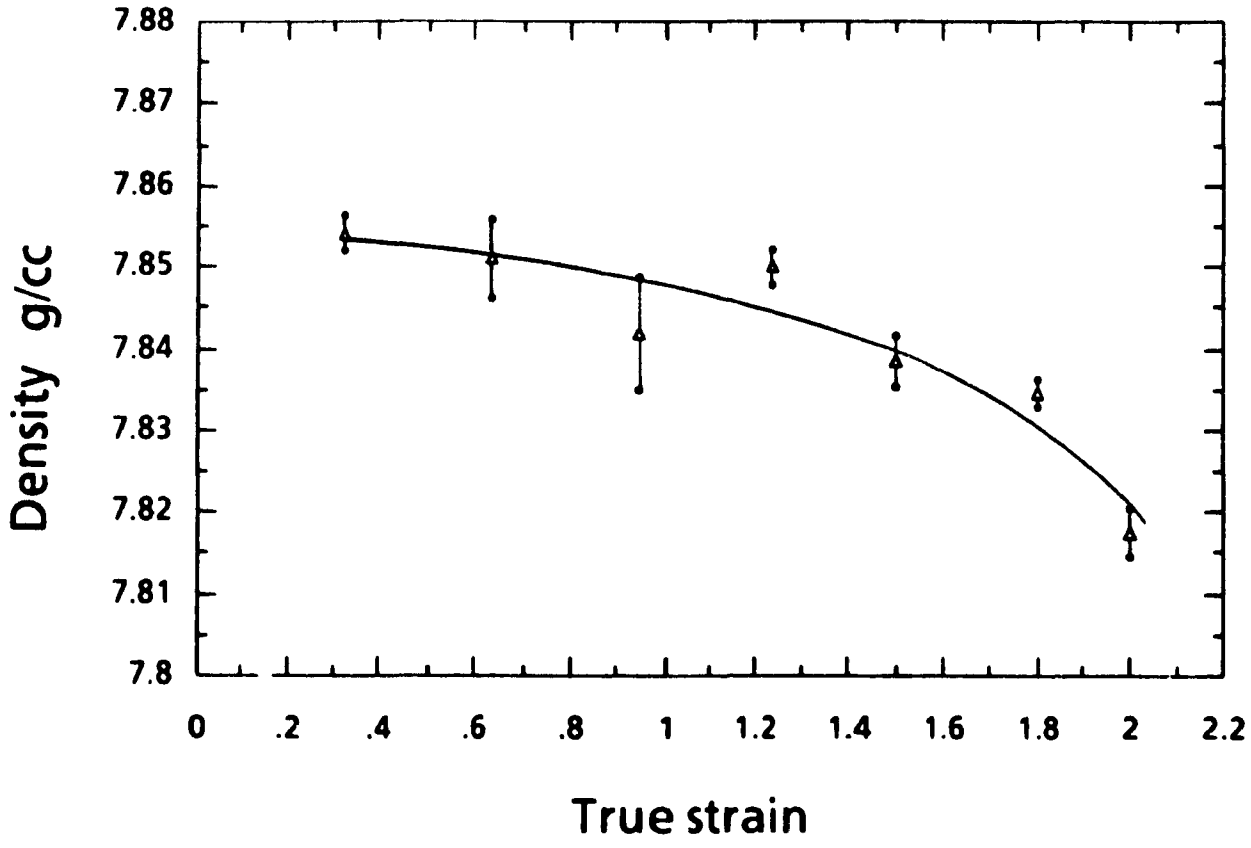

Density vs true strain
figure 24 A22671

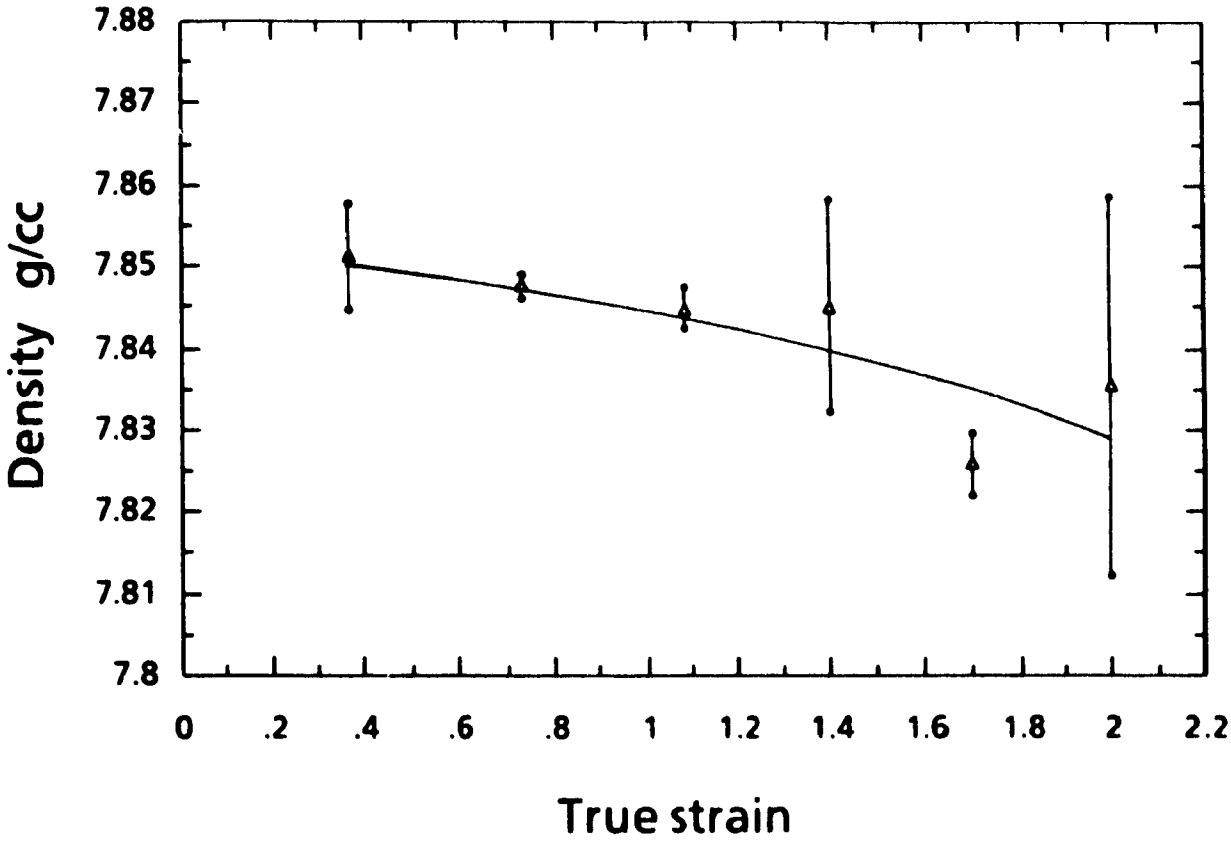

Density vs true strain
figure 25 comparison of steels

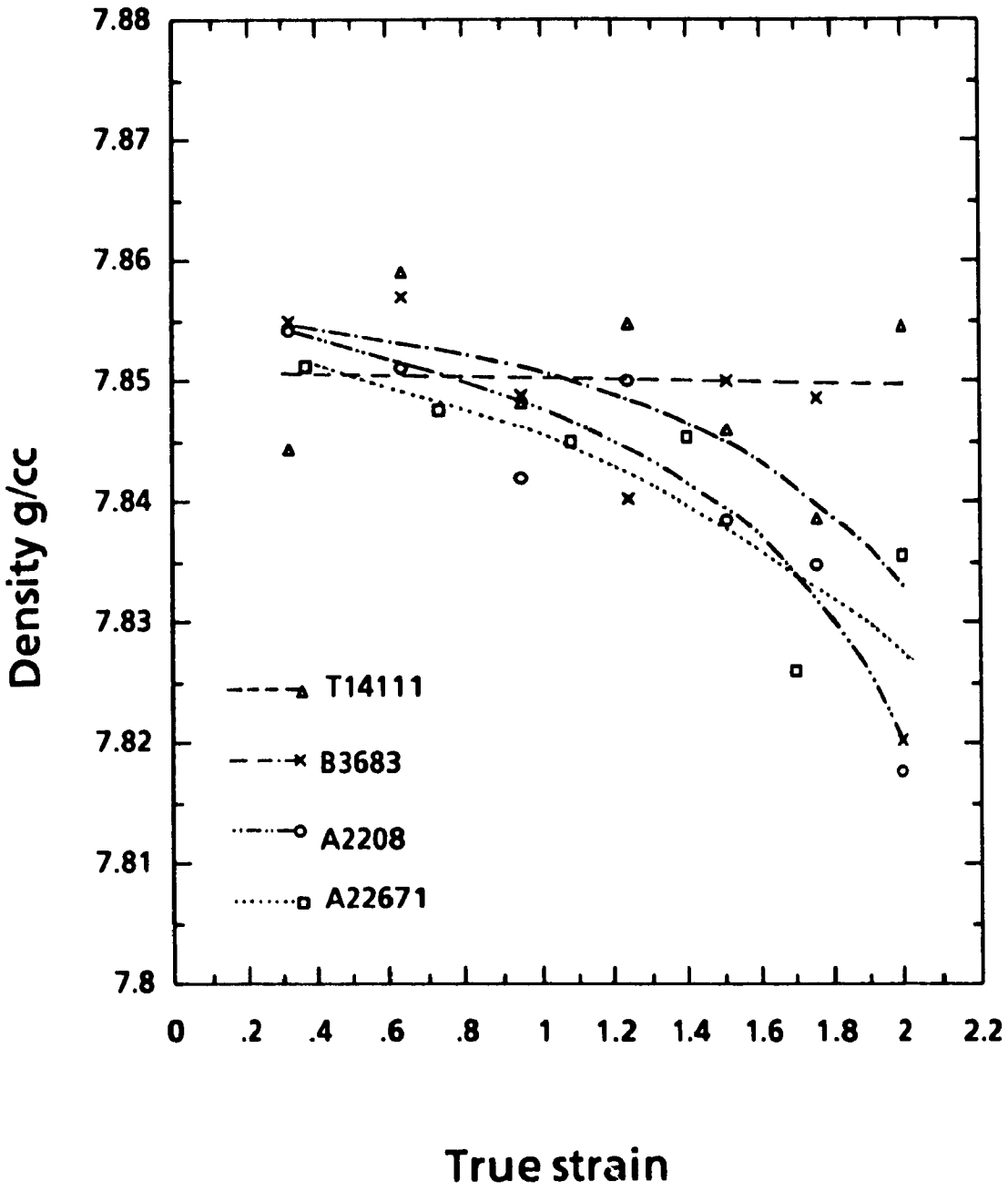

DISCUSSION OF RESULTS

Examination of table 3, and figures 17 to 19 shows that the general slopes of the true stress-strain curves were similar. Heat B3683 had the highest carbon concentration of the steels tested. The initial yield strength, after the first die, was 55 MPa greater than the softest heat, T14111. The final yield strength of heat B3683, after the last die, was 83 MPa greater than that of heat T14111. The relationship can be seen in figure 20, page 62, in which the three stress-strain curves are presented on the same axes. Reference to table 1 shows that heat T14111 had higher C, Mn and Si concentrations than heat A2208, and greater Mn and Si concentrations than B3683. In spite of this, heat T14111 was the softest steel throughout processing. It is significant that heat T14111 had the lowest copper and nitrogen content of all the steels examined.

Figure 23 on page 65 shows that a clear reduction of density has taken place as a result of straining in heat A2208. Data points presented are the average values. The variation shown is one standard deviation above and below the average. The density of A22671 exhibits a clear downward trend in figure 24, page 66. Heat B3683 shows the most scatter in the experimental results, but a general density reduction can be observed in figure 22, page 64. The graph showing the density as a function of strain for heat T14111, figure 21 presented on page 63, is the only graph which does

not show a strong reduction in density. Figure 25, page 67 is a plot of the four density curves on the same axes.

The electron micrographs, figures 12 to 15 help relate the observed changes in density to the mechanical damage which takes place during cold working. Heat B3683 was the only heat which exhibited wire breaks during processing. Figures 14 and 15 show the presence of void sheets, as described by Rogers (19). The only examples of void sheets observed were on two finished wire samples from heat B3683. Figure 15 is a micrograph of a void sheet made on a sample in close proximity to the wire break which occurred in the roll straightener. The sample photographed in figure 14 was not obtained near a wire break (AP 4).

The void sheet damage observed on heat B3683 was different in character from the voids formed on individual inclusions which had separated from the matrix during processing. Figure 12 shows a globular inclusion in heat T14111 which had separated from the metal after the first draft, at a strain of 0.32. Figure 13 shows a similar inclusion in wire which had been drawn down to the final size. After a reduction of area of 86%, and a total accumulated strain of 2.0, there does not appear to be substantially more internal damage around the inclusion than there was after the first pass. This suggests that in some cases, metal can flow to accommodate an inclusion, so that it

does not concentrate stress.

Heat A2208 exhibits the clearest reduction in density as shown in figure 23, although no wire breaks occurred during the processing of steel from this heat. The heat had the highest sulphur of the steels tested. Gladman (29) has shown that sulphides provide sites for void nucleation (AP 5).

Reference to tables 1 and 2 shows that the only chemical element which clearly distinguished heat T14111 from the other steels tested was low nitrogen, although the copper content was somewhat lower. This points to nitrogen as having the greatest effect on ductility of the elements examined.

The association of nitrogen to ductile failure is consistent with results obtained by other researchers. Dunand and Roesch (11) found that copper had very little effect on the drawability of wire. Steel with a high nitrogen content, on the other hand, exhibited internal damage and wire breaks during drawing.

Copper strengthens steel both as a substitutional alloy, and through a precipitation strengthening effect. The solubility of copper in steel at room temperature is of the order of 0.25% (25). Irani et al. (25) have reported that copper is responsible for a 13.8 MPa increase in both the yield strength and tensile strength of low carbon steel. Their work was based on steels in which the copper

concentration was in excess of 0.60%. At this copper level, copper precipitates probably contributed to the increase in strength.

At the levels of copper found in the experimental steels, and in those used by Dunand and Roesch (11), it would be reasonable to say that the effect of copper would be difficult to separate from the scatter associated with mechanical testing methods.

The effect of tin, in the concentrations normally found in commercial steels is so small, it is also difficult to separate the effect of tin from the normal scatter observed when performing tensile tests (26).

Nitrogen is an interstitial alloying element, and has an effect similar to that of dissolved carbon (27). The solubility of carbon in steel is less than 200 ppm at room temperature (7), so the concentration of nitrogen encountered in the steels studied is significant in comparison to the concentration of dissolved carbon. Carbon present in the steel in excess of the solubility limit will be in the form of the intermetallic compound Fe_3C, and not in solid solution.

The effect of interstitial carbon and nitrogen on yield and tensile strength is linear. The effect on yield strength is a 0.50 MPa increase for each ppm of dissolved N or C. The effect on tensile strength is an increase of 0.59 MPa for

each ppm of interstitial N or C (27).

Nitrogen and soluble carbon have a great deal of mobility in solid solution, due to their interstitial positions in the lattice. The strengthening mechanism of interstitial N and C is through the formation of a pinning atmosphere around dislocations (7). This atmosphere impedes the motion of dislocations, the motion of which are responsible for plastic yielding.

The unpinning of dislocations from interstitial atmospheres is responsible for the yield drop which can be observed during tensile testing. The yield drop is an example of flow softening. Flow softening can lead to flow localization (30).

It can be theorized that the flow localization responsible for the void sheets observed in the high nitrogen heat, B3683, is caused by the yield drop phenomenon. At room temperature, it takes several days for a cold worked steel to strain age, and develop a yield drop. As the storage temperature increases, the strain ageing time is reduced.

During wire drawing operations, temperatures in the die will be of the order of 200 °C. At these temperatures, the nitrogen may have sufficient mobility to pin dislocations as the wire moves from one die to the next. If this occurred,

then the yield drop flow softening mechanism could account for flow localization, as well as for the void sheets which were observed in the samples. One of the conditions of plastic instability is flow localization, void sheets being the result of constrained, localized flow.

This theory accounts for the observation that wire breaks can be reduced by lowering the drawing speed, or by reducing the nitrogen content of the steel. An increase in the drawing speed will raise the wire temperature. For a given nitrogen content, there is a critical temperature above which there is sufficient nitrogen mobility for dislocations to become pinned between wire drawing dies. Once this begins, flow localization will occur, leading to the formation of void sheets, and the failure of the wire. On the other hand, if drawing speed was constant, a steady state temperature would be reached, which would be a function of the drawing speed, the type of steel, and the specific wire drawing equipment used. If, under those steady conditions, steels with increasing nitrogen concentrations were processed, a nitrogen level would be reached at which dislocation pinning could occur between dies. Once again, flow localization and wire failure would occur.

CONTRIBUTION TO ORIGINAL KNOWLEDGE

A number of researchers have used density measurement techniques to study the effects of cold work on metals. Rogers and Coffin (12) used the technique to study metal to die friction. Coffin and Rogers (13) also studied the effect of imposed hydrostatic pressure on internal damage. Moussy and Quennevat (28) have related changes in density to the inclusion content of steels. Gladman (29) did related work, but concentrated specifically on sulphide inclusions. Dunand and Roesch (11) used precision density to study the relationship of residual elements, and nitrogen concentrations to wire drawability.

The research described in this thesis has extended the methods previously described, to commercially drawn wire. While previous researchers made use of apparatus of the laboratory, single draft type, this author was able to apply precision density change measurement methods to steels processed at commercial speeds on a multiple die drawing machine.

Using an eight pass, low die angle arrangement, results were obtained which are similar to those reported by Dunand and Roesch (11), using a high angle die. A high angle die was employed because it exaggerates the internal damage, with the aim of reproducing the effects of high speed multiple

pass drawing. The present work contributes to original knowledge by extending laboratory test methods to commercial operations, thus confirming the more basic results of earlier workers.

CONCLUSIONS

The mobility of free nitrogen, and the ability of free nitrogen to pin dislocations probably account for the effect that drawing rate has on wire breaks.

The influence of nitrogen on the drawability of low carbon steel is greater than the effect of the other metal residual elements considered. The reduction in drawability is caused by the presence of interstitial nitrogen in the steel. The addition of nitride formers, such as boron, improves the drawability of low carbon steel by removing nitrogen from its interstitial positions, and locking it in place as an intermetallic compound.

This may account for the popularity of aluminum killed and silicon aluminum killed steels. These steels are in demand for severe cold forming applications, such as tubular rivets, and spark plug bodies. The tensile testing of steels containing aluminum does not reveal mechanical properties which differ significantly from those of silicon killed steels with similar chemistries. Steels which contain aluminum do, however, show a superior ability to withstand severe forming operations without failure. The presence of aluminum as a nitride former could account for the difference, by its ability to combine with interstitial nitrogen.

Aluminum killed, and silicon aluminum killed steels are inherently cleaner than silicon killed steels. Sulphur levels are typically an order of magnitude lower, due to the effect of reduced dissolved oxygen on the partitioning of sulphur between liquid steel and slag. The reduction in sulphides, combined with the removal of interstitial nitrogen, will provide improvements in ductility which will only be observed after large amounts of strain, and high deformation rates, such as those encountered during commercial forming operations.

The results obtained during these investigations may provide some relief to steel producers who are facing increasing chemical restrictions on their products. Historically, steel was produced in blast furnaces, using open hearth furnaces or pneumatic processes to convert the iron into steel. These operations produce a low nitrogen steel, and use a small percentage of scrap. The steel produced was relatively low in tramp elements, as well as nitrogen.

When electric furnace based operations began to compete in the wire market, their performance did not match that of steel produced by traditional, iron ore based steelmakers. An obvious reason for this lack of performance seemed to be

the tramp element content of the steel. Nitrogen was not as obvious a problem as metallic tramp elements, because it cannot be measured accurately on most emission spectrometers.

Electric furnaces produce a steel which is higher in nitrogen than a steel produced using a pneumatic converter. When residual restrictions became common, electric furnace operators were forced to use pre-reduced pellets, or pig iron. Both these sources of iron result in more bath agitation, which helps reduce nitrogen. The resulting steel was lower in tramp element concentration, with a greater probability of having low nitrogen.

The results of this investigation show that there is a possibility that a wire drawing operation that produces its own steel may be able to develop specifications which would contain nitrogen restrictions or include nitride formers, but allow higher metallic tramp element concentrations. This could produce a deformable steel, but at the same time allow the use of more economical, higher residual scrap.

REFERENCES

1) Pflaum,D. "Residual Problems and The Scrap Industry" Residual and Unspecified Elements in Steel, ASTM STP 1042, A.S.Melilli and E.G. Nisbett, Eds, American Society for Testing Materials, Philadelphia, 1989, pp 11-25

2) Iverson,F. "Electric Furnaces in the US" Iron and Steelmaker, May 1983 pp 44-46

3) McCallum,R. "Power Demand Control at Eastern Steelcasting" Submitted as a partial requirement of course 605 at Concordia University.

4) Glasgal,B. "Some Practical and Economic Aspects of Residual Element Control in Engineered Bar Products", Residual and Unspecified Elements in Steel, ASTM STP 1042, A.S.Melilli and E.G.Nisbett, Eds.,American Society for Testing Materials, Philadelphia, 1989, pp 26-37

5) AISI Iron and Steel Statistics, published by American Iron and Steel Institute, Washington, December 1990

6) Purcino,E. Cetlin,P. "The Drawability of Carbon Steels" Wire Industry, April 1991, pp 201 - 203

7) Dieter,G. "Mechanical Metallurgy" Third edition, McGraw Hill Book Company 1986 New York

8) Avitzur,B. "Handbook of Metal Forming Processes" Wiley and Sons, 1983

9) Berner,D. "Die Design and Modern Finishing Techniques for the Improvement of Wire Quality" Proceedings of 15th Wiretech Conference, Society of Manufactureing Engineers (SME) and Wire Association International April 1990, Philadelphia

10) Wright,R. "Mechanisms of Wire Breaks" Proceedings of 1990 Wiretech Conference, Philadelphia. Sponsored by SME, Dearborn Michigan.

11) Dunand,M. Roesch,L. "Influence des éléments résiduels sur le tréfilabilité d'aciers extra-doux" Revue de métallurgie 84e année - No 6 Juin 1987

12) Rogers,H., Coffin,L. "An Analysis of the Effect of Friction on Sheet Drawing" International Journal of Mechanical Science, Pergamon Press, 1971 Vol 13 pp 141-155

13) Coffin,L. Rogers,H. "Influence of Pressure on the Structural Damage in Metal Forming Processes" Transactions of the ASM Volume 60, 1967 pp 672-686

14) Rowe,G. "An Introduction to the Principles of Metalworking" Edward Arnold Publishers Ltd., 1965

15) Hill,R. "The Mathematical Theory of Plasticity" Oxford at the Clarendon Press. 1985 paperback edition

16) Wistreich,J. "Investigation of the Mechanics of Wire Drawing" 1955 proceedings: The Institution of Mechanical Engineers, Vol 169 pp 654-665

17) Avitzur,B. "Metal Forming: Processes and Analysis" McGraw Hill, New York, 1968

18) Avitzur,B. "Analysis of Central Bursting Defects in Extrusion and Wire Drawing" Journal of Engineering for Industry, Transactions of the ASME Feb. 1968 pp 79-91

19) Rogers,H. "The fundamental aspects of Deformation Processing" Fundamentals of Deformation Processing, proceedings of the 9th Sagamore Army Materials Research Conference, 1962. Syracuse University Press, 1964

20) Dillinger,L. Leco Instruments Laboratory St.Joseph,Michigan Private Communication.

21) Moussy,F. Quennevat,C. "Le Polissage par bombardement ionique: technique et applications" Traitement Thermique Nov. 1986 pp 31-37

22) Moussy,F. "Microstructure, endommagement et rupture ductile" Mémoires et Etudes Scientifiques Revue de Métallurgie, avril 1987 pp 205-222

23) Rhodorsil Huiles Reference X 03-04 B May 1979 Société Chimique de la Courneuve B.P. 151 45 Quai Lucien Lefranc 93304 Aubervilliers Cedex, France

24) Moussy,F. Private Communication

25) Irani,J. Dulieu,D. Tither,G. "Role of Copper in Low-Alloy Steels" ISI special report 114,1968 pp 75-89

26) Stephenson,E. "Tin and Properties of Steel" Journal of Metals, March 1974 pp 48-51

27) Pickering Gladman,T. "Strength of Carbon Steels" Metallurgical Development of Carbon Steels, ISI special Report, 1981

28) Moussy,F. Quennevat,C. "Effect of Inclusions on Steel Properties: A New Approach" Proceedings of the 25th Confrence of Americal Metallurgists, AIME Toronto, 1986

29) Gladman,T. "Cavitation at Sulphides during Deformation" Sulphide Inclusions in Steel Symposium, 1974. American Society for Metals Technology Press.

30) Semiatin,S. Jonas,J. "Formability and Workability of Metals: Plastic instability and flow localization" American Society for Metals, 1984

APPENDIX

1) The velocity field model referred to (8,18) is based on geometric principles. The model is capable of predicting conditions under which there is a danger of central bursting, but does not address the problem of why central bursting will not occur in all cases once critical limits, such as die half angle and reduction of area are exceeded.

It could be theorized that in an ideal material, upon which the velocity field theory is based, a stress applied to the surface during drawing will be transmitted to the centre, based upon the geometric calculations described on pages 11 to 13 of this thesis. In a real material, on the other hand, due to physical circumstances, such as dislocation pile ups, stress will be concentrated near the surface of the sample, and the plastic deformation zone will not extend to the centre line. Under this condition, central bursting will develop, as described in pages 15 to 17, in order to accommodate the velocity differences between the die entrance and exit, which are no longer separated by a continuous deformation zone.

2) The elements selected for study in the thesis, as shown in table 2, page 49 were chosen because they are the elements most often restricted by the customers of Ivaco Rolling Mills, which are not intentionally added to steel in the form of ferro alloys.

3) Tensile testing was performed on three of the four steels tested. Tensile testing of the wire after each die was not conducted on samples from heat A22671 because insufficient material was collected to perform both tensile testing and precision density measurements. This sampling error was corrected during subsequent experiments.

4) The expression "Void sheet" is from Rogers (19), and does not refer to the geometric shape of the defect. The defect was described as a void sheet, because no inclusions or chemical segregation could be seen in the vicinity of the defect during SEM observation.

5) It is assumed that the density reduction observed was caused by the decohesion of sulphide type inclusions. The amount of inclusions present in heat A2208 would have been greater than in the other steels tested, due to the high sulphur content of that heat. The nitrogen content may not have been great enough to cause flow localization during wire drawing, hence there were no breaks. The lower density does, however, show that the wire produced was of inferior quality to, for example wire produced from heat T14111, in which there was not a noticeable drop in density.